Atmos. Meas. Tech. Discuss., 8, 11077–11138, 2015
www.atmos-meas-tech-discuss.net/8/11077/2015/
doi:10.5194/amtd-8-11077-2015

Atmospheric Measurement Techniques Discussions
Open Access

This discussion paper is/has been under review for the journal Atmospheric Measurement Techniques (AMT). Please refer to the corresponding final paper in AMT if available.

The new sun-sky-lunar Cimel CE318-T multiband photometer – a comprehensive performance evaluation

A. Barreto[1,2], E. Cuevas[1], M. J. Granados-Muñoz[3,4], L. Alados-Arboledas[3,4], P. M. Romero[1], J. Gröbner[5], N. Kouremeti[5], A. F. Almansa[1,2], T. Stone[6], M. Sorokin[7], B. Holben[7], M. Canini[2], and M. Yela[8]

[1]Izaña Atmospheric Research Center, Meteorological State Agency of Spain (AEMET), Spain
[2]Cimel Electronique, Paris, France
[3]Department of Applied Physics, University of Granada, Granada, Spain
[4]Andalusian Institute for Earth System Research, IISTA-CEAMA, University of Granada, Junta de Andalucía, Granada, Spain
[5]Physikalisch-Meteorologisches Observatorium Davos and World Radiation Center (PMOD/WRC), Davos, Switzerland
[6]US Geological Survey, Flagstaff, USA
[7]NASA/Goddard Space Flight Center, Greenbelt, USA
[8]Instrumentation and Atmospheric Research Department, National Institute for Aerospace Technology (INTA), Madrid, Spain

Received: 18 September 2015 – Accepted: 21 October 2015 – Published: 28 October 2015

Correspondence to: A. Barreto (cimel1@aemet.es)

Published by Copernicus Publications on behalf of the European Geosciences Union.

Abstract

This paper presents the new photometer CE318-T, able to perform daytime and night-time photometric measurements using the sun and the moon as light source. Therefore, this new device permits to extract a complete cycle of diurnal aerosol and water vapor measurements valuable to enhance atmospheric monitoring. In this study we have found significantly higher triplets precision when comparing the CE318-T master and the Cimel AErosol RObotic NETwork (AERONET) master (CE318-AERONET) triplets as a result of the new CE318-T tracking system. Regarding the instrument calibration, a new methodology to transfer the calibration from a master (Sun Ratio technique) is presented and discussed. It allows us to reduce the previous complexities inherent to nocturnal calibration. A quantitative estimation of CE318-T AOD uncertainty by means of error propagation theory during daytime revealed AOD uncertainties (u^{D}_{AOD}) for Langley-calibrated instruments similar to the expected values for other reference instruments (0.002–0.009). We have also found u^{D}_{AOD} values similar to the values reported in sun photometry for field instruments (~ 0.015). In the case of nighttime period, the CE318-T estimated uncertainty (u^{N}_{AOD}) is dependent not only on the calibration technique but also on illumination conditions and the instrumental noise. These values range from 0.011–0.019 for Lunar Langley calibrated instruments to 0.012–0.021 for instruments calibrated using the Sun Ratio technique.

A subsequent performance evaluation including CE318-T and collocated measurements from independent reference instruments has served to assess the CE318-T performance as well as to confirm its estimated uncertainty. Daytime AOD evaluation performed at Izaña station from March to June 2014, encompassed measurements from a reference CE318-T, a CE318-AERONET master, a Precision Filter Radiometer (PFR) and a Precision SpectroRadiometer (PSR) prototype, reporting low AOD discrepancies between the four instruments (up to 0.006). The nocturnal AOD evaluation was performed using CE318-T and star photometer collocated measurements and also by means of a day/night coherence transition test using the master CE318-T and the

CE318 daytime data from the CE318-AERONET master. Results showed low discrepancies with star photometer at 870 and 500 nm channels (≤ 0.013) and differences with AERONET daytime data (1 h after and before sunset and sunrise) in agreement with the estimated u^{N}_{AOD} values at all illumination conditions in case of channels within the visible spectral range, and only for high moon's illumination conditions in case of near infrared channels.

Precipitable water vapor (PWV) validation showed a good agreement between CE318-T and Global Navigation Satellite System (GNSS) PWV values for all illumination conditions, within the expected precision for sun photometry.

Finally, two case studies have been included to highlight the ability of the new CE318-T to capture the diurnal cycle of aerosols and water vapor as well as short-term atmospheric variations, critical for climate studies.

1 Introduction

The energy from the Sun constitutes the driving force of the Earth's climate, but not all of the solar energy that incides at the top of the atmosphere reaches the surface. In this respect, aerosols play an important role in the Earth's radiation budget, directly modifying the energy balance by the scattering/absorption of the solar radiation, and indirectly through their impact on cloud formation and properties (Foster et al., 2007; Kaufman et al., 2002; Myhre, 2009). There is also a semi-direct aerosol effect associated with the absorption of solar radiation by aerosols which could potentially modify cloud properties (Kaufman et al., 2002). However, the high spatial/temporal variability of aerosols and the high complexity of aerosols in the atmosphere make the task of quantifying their climate effect difficult. Indeed, according to the IPCC report (Stocker et al., 2013), aerosols dominate the uncertainty associated with the total anthropogenic driving of climate change. This report estimated a global and annual direct radiative forcing effect of anthropogenic aerosols of $-0.35\,\mathrm{W\,m^{-2}}$, with an uncertainty ranging from -0.85 to $-0.15\,\mathrm{W\,m^{-2}}$. The total aerosol radiative effect including aerosol-cloud interactions

AMTD
8, 11077–11138, 2015

was estimated as a radiative forcing of −0.9 (−1.9 and −0.1) $W m^{-2}$. Notable recent advances in the last decades in the understanding of atmospheric aerosols have substantially reduced the uncertainty in the total direct aerosol effect on the Earth's climate (Myhre, 2009). The combination of aerosol satellite and ground-based measurements have resulted in a remarkably increased knowledge about aerosol geographical distribution, concentration and microphysical properties, but there are still large uncertainties in individual radiative forcing for several of the aerosol components, such as black carbon particles, organic carbon, or nitrates (Myhre, 2009). This uncertainty reflects how challenging it is to quantify the aerosol radiative forcing and highlights the need to adequately determine their nature and spatial/temporal variability on both regional and global scales.

At present, there are several global or regional networks established during the last two decades based on measurements at ground level; the globally distributed AErosol RObotic NETwork (AERONET) is one of the most important networks for passive long-term aerosols monitoring (Holben et al., 1998, 2001). This global sun photometer network offers aerosol optical, microphysical and radiative properties using the standard sun photometer CE318-N as reference instrument (hereinafter referred to as CE318-AERONET), in addition to real time data reception accessible for the scientific community (Holben et al., 2001). Another reference network for aerosol monitoring is the Global Atmosphere Watch (GAW) network, using the Precision Filter Radiometer (PFR) as reference instrument (Wehrli, 2000, 2005). The PFR instrument was developed by the World Optical Depth Research and Calibration Center (WORCC) that was established in 1996 by World Meteorological Organization (WMO), assigned as the reference center for spectral radiometry to determine AOD (WMO, 2003). However, in spite of the high temporal and spectral resolution provided by these networks, the sun photometry provides aerosol information restricted to the daylight period and column-averaged. These are the two most important limitations of solar photometry, which prevent the existence of aerosol observations with the required temporal resolution for climate studies. This problem is especially challenging at high latitude locations, due to the

AMTD
8, 11077–11138, 2015

extended periods of darkness at wintertime, which significantly limits the information we have to better understand this fragile climate system.

Several studies in the literature are focused on the estimation of AOD at nighttime by means of star photometry (Ansmann et al., 2001; Herber et al., 2002; Pérez-Ramírez et al., 2008a, 2011; Baibakov et al., 2015). Although this technique is able to determine AOD with similar accuracies to sun photometry (expected errors in AOD of ~ 0.02 for $\lambda < 800$ nm and ~ 0.01 for $\lambda > 800$ nm) (Pérez-Ramírez et al., 2011), the important operational difficulties and the complexities of such large-aperture systems needed to collect the weak star light make stellar measurements still limited in use, especially for large scale networks such as AERONET. Recently, Barreto et al. (2013a, b) presented a new photometer prototype (CE318-U), similar to the CE318-AERONET reference instrument, with a prototype four-quadrant detector able to perform lunar measurements to characterize aerosols and water vapor at nighttime. These authors showed that this new CE318-U instrument permits to derive, in combination with the current CE318-AERONET, a continuous sequence of diurnal aerosol concentrations. This instrument was able to perform nocturnal measurements under moon illumination greater than 50 % and therefore it was able to cover 50 % of the moon cycle, providing the opportunity to significantly extend the continuity of existing observations.

The use of active remote measurements such as advanced ground-based lidars systems prevents the last two handicaps of sun photometry, providing daytime and nighttime information about the atmospheric vertical structure. As a result, this technique has proven to be very effective in the characterization of aerosols in high latitude regions (Baibakov et al., 2015; Tomasi et al., 2015; Hoffmann et al., 2009). Lidars allow us to determine vertical profiles of aerosol optical properties and estimate some microphysical properties (only using multiwavelength Raman Lidars), but some physical or mathematical constrains are necessary in the inversion algorithm. The synergy lidar-sunphotometers is currently implemented and successfully checked (Fernald, 1984; Klett, 1985; Cuesta et al., 2008; Chaikovsky et al., 2012; Lopatin et al., 2013) to minimize the uncertainties of these assumptions when inverting the lidar signals using the common Klett-Fernald-Sasano technique (Fernald, 1984; Klett, 1985; Sasano et al., 1985). It also serves to reduce uncertainties in microphysical properties retrieval using multiwavelength lidars (Pahlow et al., 2006; Tesche et al., 2008). Some examples in the literature of the potential of this combined lidar-photometer observations are the numerical tool LIRIC (LIdar/Radiometer Inversion Code), developed by Chaikovsky et al. (2012), or GARRLiC (Generalized Aerosol Retrieval from Radiometer and Lidar Combined data) method, introduced by Lopatin et al. (2013) and tested by Wagner et al. (2013) and Granados-Muñoz et al. (2014). More recently, Barreto et al. (2014a) and Baibakov et al. (2015) showed the improvement in the synergetic retrieval of AOD at nighttime using a combination of Lidar and lunar-photometer (CE318-U) in the first case, and by means of Lidar and star photometer in the second case.

In this work we present the new photometer CE318-T (Sect. 2), which combines the features of the extensively used CE318-AERONET standard model (Holben et al., 1998) with the ability to perform nocturnal measurements of the prototype CE318-U, described in Barreto et al. (2013a, b). The instruments CE318-T were deployed at Izaña Atmospheric Observatory (IZO) and Granada stations. IZO is a high altitude site while Granada is an urban station. These sites are presented in Sect. 3. The instruments as well as the supporting information used to evaluate the CE318-T performance and the lunar irradiance model are shown in Sect. 4. The instrument's calibration is described and assessed in Sect. 5.1, where the new Sun Ratio technique is introduced to perform the calibration transference from a master for both day and nighttime conditions using only daytime measurements. The absolute calibration of this instrument is also shown as a combination of the usual Langley Method for daytime and the Lunar Langley Method for nighttime. In Sects. 5.2 and 5.3 we detail the methodology to obtain AOD, Angström's exponent (AE) and PWV using CE318-T. Section 6 describes a quantitative estimation of CE318-T AOD uncertainty. In Sect. 7 we present the assessment of the Sun Ratio calibration method (Sect. 7.1) and the evaluation analysis of CE318-T AODs carried out by comparison of AODs extracted at daytime period from four different independent instruments (CE318-T master, CE318-AERONET master, PFR and Precision SpectroRadiometer -PSR-) (Sect. 7.2) and, for nighttime, using CE318-T measurements with collocated star photometer observations (Sect. 7.3). We have extended the evaluation analysis through a day/night coherence test transition using CE318-AERONET daytime and CE318-T AOD information (Sect. 7.4). Daytime and nighttime CE318-T PWV measurements at IZO were validated against Global Navigation Satellite System (GNSS) and AERONET data in Sect. 7.5. Two demonstration case studies (Sect. 8) showed the ability of the instrument to monitor short-scale atmospheric processes. Finally, the main conclusions of the present study are summarized in Sect. 9.

2 Instrumentation – the new sun-sky-lunar Cimel CE318-T

The new sun-sky-lunar Cimel CE318-T photometer has been developed by the French company Cimel Electronique improving the tracking precision in order to perform both daytime and nighttime (lunar) measurements and providing additional and enhanced operational functionalities compared with the standard sunphotometer CE318-AERONET, extensively described in Holben et al. (1998). The CE318-T is based on a new control unit and a new four-quadrant system in the sensor head.

The CE318-T is based on the former prototype CE318-U, described in Barreto et al. (2013a, b), which presents higher signal-to-noise ratios (better than 60 dB) to capture not only the daytime radiation from the sun but also the limited energy during nighttime reflected by the moon, and therefore is able to provide valuable information of aerosols and water vapor at nighttime.

Similarly to the standard CE318-AERONET, the new CE318-T performs measurements at an approximate field of view of 1.29° at ten nominal wavelengths of 1020, 937, 870, 675, 500, 440, 380 and 340 nm, using a silicon photodiode detector, as well as additional measurements at 1020 and 1640 nm using an InGaAs detector. Due to the low signal in the UV channels at night, AOD cannot be obtained and therefore UV information is restricted to the daylight period.

AMTD
8, 11077–11138, 2015

This new instrument performs three different measurement types: spectral direct sun and direct moon irradiance measurements to obtain aerosol and water vapor content, and spectral sky radiances to infer aerosol properties from inversion during daytime period. This is the reason for applying the term “triple” to this new Cimel photometer. As in the standard AERONET version, the CE318-T takes a sequence of three measurements (triplet) every 30 s at each wavelength. The triplet value is defined as the maximum minus minimum divided by the mean value of these three consecutive measurements. It means that each triplet represents the normalized range of these three consecutive measurements. At this moment, the triplet information is used to detect and remove clouds as well as to check the instrument’s stability until a new operative cloud screening is applied.

Among the new features of this new instrument (CE318-T) we highlight the following:

- New tracking system. The new four-quadrant detector in the sensor head is designed to track both the Sun and the Moon. The tracking firmware has been optimized to provide robust moon tracking even in presence of nearby clouds or night-time light pollution. The new control box uses micro-stepping technology to control the robot. All movements are smoothed and full step shocks are eliminated. The pointing resolution is improved to 0.003° on both axes. The robot is held in position between each movement to avoid unwanted movements caused by wind or cables. With all of these new features, the new tracking system is expected to improve measurement precision at daytime compared to the CE318-AERONET version.

- The control box is equipped with a powerful microprocessor, an internal 4 Mb flash memory, and an on board SD Card that avoids any loss of data.

- A single powerful firmware includes all usual scenarios for any of the four CE318-T models: standard, polarized, sea-prism and BRDF. It also includes new scenarios like hybrid scenario (for sky measurements with larger scattering angles) and curvature cross from ±3 to ±7.5° (for improved cloud screening at daytime).

AMTD

8, 11077–11138, 2015

- Data are stored and transferred with 32 bits. As a result, previous digital gains have been eliminated.
- The instrument is designed to run (both daytime and nighttime) with its usual solar panel, for better protection against lightning effects. The internal battery has been suppressed in order to simplify operations, and the power consumption has been reduced. The local interface is improved with a robust touch keyboard and a large backlit graphic LCD display.
- The atmospheric pressure is measured at each group of scenarios by a barometer integrated in the connector panel. The control box is also equipped with inputs to connect a pyranometer and is designed to support a SDI12 bus.
- The control box is equipped with a GPS receiver for improved time synchronization and automatic localization.
- It supports communications through local Serial, local USB and local radio, and remotely through GPRS mobile phone with automatic transfer via FTP or Web site. For isolated locations, it supports communication through satellite DCP with fully automated DCP configuration.

3 Measurement sites

The Izaña Atmospheric Observatory (http://izana.aemet.es) is a high mountain atmospheric monitoring station located at 2373 m a.s.l. in Tenerife, Canary Islands, Spain (28.31° N; 16.49° W). It is managed by the Izaña Atmospheric Research Center (IARC) from the State Meteorological Agency of Spain (AEMET). High quality atmospheric measurements are carried out at IZO since it is normally located above a strong and quasi-permanent subsidence temperature inversion typical of the subtropical regime which prevents pollution from lower parts of the island. Clear skies and high atmospheric stability make IZO a suitable site for atmospheric monitoring and calibration

Discussion Paper | Discussion Paper | Discussion Paper | Discussion Paper |

AMTD

8, 11077–11138, 2015

The new sun-sky-lunar Cimel CE318-T multiband photometer

A. Barreto et al.

Title Page
Abstract Introduction
Conclusions References
Tables Figures
◀ ▶
Back Close
Full Screen / Esc
Printer-friendly Version
Interactive Discussion

activities under free tropospheric conditions. Moreover, this station also allows us to measure under Saharan Air Layer (SAL) conditions (Rodríguez et al., 2011, 2015; Cuevas et al., 2013, 2015; Barreto et al., 2014b) which is an advantage to characterize photometers in a wide range of AOD and AE values. This station is a member of the WMO-GAW programme and is one of the two direct-sun calibration sites of the AERONET network (Holben et al., 1998). IZO is also a WMO Commission for Instruments and Methods of Observation (CIMO) Testbed for Aerosols and Water Vapor Remote Sensing Instruments.

Granada station (37.16° N, 3.60° W, 680 m a.s.l) is an EARLINET (Pappalardo et al., 2014) and AERONET station, managed by the Atmospheric Physics Group (GFAT) at the Andalusian Institute for Earth System Research (IISTA-CEAMA). The station is located in the south-east of Spain in a non-industrialized metropolitan area surrounded by mountains. Its aerosol climatology is dominated by Atlantic air masses, usually associated with low aerosols conditions, air masses from Europe and the Mediterranean basin, with more influence of anthropogenic particles, and also an important influence of mineral dust from the African continent (Valenzuela et al., 2012) detected in lofted aerosol layers in the free troposphere that can affect the Boundary Layer (Guerrero-Rascado et al., 2009; Navas-Guzmán et al., 2013; Bravo-Aranda et al., 2015). The experimental site is also affected by anthropogenic particles and dust resuspension from local aerosol sources (Lyamani et al., 2010, 2012; Titos et al., 2014).

4 Instruments and supporting information

4.1 Independent AOD measurements

Several CE318-T instruments have been installed at IZO since 2013. The master instrument was in operation since December 2013, but only information from March 2014 to present can be used to characterize its performance. Another instrument, referred to as secondary, was installed from March to June 2014. Coincident information extracted

AMTD
8, 11077–11138, 2015

from these paired instruments have been used to validate the new calibration transference technique developed for CE318-T. Later, this secondary instrument was sent to Granada station, where it was in operation during August 2014.

In this work we have used ancillary data collected at IZO from Cimel AERONET instrument. AERONET Version 2 Level 2.0 AOD data was retrieved from the IZO master #244 (http://aeronet.gsfc.nasa.gov). This information is quality-assured following the AERONET protocol (Holben et al., 1998). We have also used AERONET Version 2 Level 1.5 not quality assured for data collected in 2015.

A 4-wavelength GAW PFR developed by the WORCC of the PMOD World Radiation Center (http://www.pmodwrc.ch/worcc/index.html) is in operation at IZO since July 2001. This instrument provides AOD at 367.6, 412.1, 501.0 and 863.1 nm. The PFR instrument of IZO is directly linked with WORCC-WMO AOD reference triad of PFRs that operate at WORCC. During April, May and June, 2014, a PSR prototype (Gröbner et al, 2012) was running at IZO, providing coincident measurements with PFR, CE318-AERONET and CE318-T. This spectroradiometer is designed to measure direct solar irradiance between approximately 300 and 1020 nm with a resolution varying between 1.4 and 6 nm over the wavelength range.

The final part of the AOD evaluation procedure involves CE318-T measurements performed at Granada station. Nighttime AOD information was obtained using the EXCALIBUR star photometer (Astronómica S. L.) which belongs to IISTA-CEAMA. More details of this system can be found in Pérez-Ramírez et al. (2008b, 2012a). This instrument acquires direct star irradiances at 380, 436, 500, 670, 880, 940 and 1020 nm using a Schmid-Cassegrain telescope and a CCD camera as a detector device. Periodical calibrations of the star photometer are performed at the high mountain station Calar Alto (37.2° N, 2.5° W, 2168 m a.s.l.), following the calibration technique described in Pérez-Ramírez et al. (2011). The instrument has been used both to follow day-night time AOD evolution (Pérez-Ramírez et al., 2012b) and to retrieve aerosol microphysical properties (Pérez-Ramírez et al., 2015).

AMTD
8, 11077–11138, 2015

Finally, we have used in this work vertical aerosol backscatter information extracted from a Micropulse Lidar (MPL), MPL-3 (SES Inc., USA) system (Spinhirne et al., 1995). This instrument has been operating at Santa Cruz de Tenerife station (28.5° N, 16.2° W; 52 m a.s.l.) since January 2005 and it is currently in operation within NASA/MPLNET network (http://mplnet.gsfc.nasa.gov). It is co-managed by the National Institute for Aerospace Technology (INTA, Spain) and the IARC. Further information about MPL and the calibration techniques can be found in Campbell et al. (2002) and in Welton and Campbell (2002).

4.2 Independent PWV measurements

For PWV intercomparison study we have used, in addition to AERONET level 2.0 PWV measurements, a LEICA GRX1200GGPRO GNSS receiver which belongs to the Spanish National Geographical Institute (IGN), operating at IZO (IZAN station, IERS code 31309M002) within the European Reference Frame network (EUREF, Bruyninx, 2004) since July 2008. This instrument is part of the EUMETNET (Network of European Meteorological Services) GNSS water vapor programme (E-GVAP). It provides instantaneous Zenith Total Delay (ZTD) values every 15 min (GNSS ultra-rapid orbits) by applying the Bernese software version 5.0 (Dach et al., 2007), meanwhile the Zenith Hydrostatic Delay (ZHD) is calculated at IZO with the actual surface pressure at the station, measured with a high-precision SETRA 470 barometer. The methodology to convert ZWD data to PWV is described in Romero et al. (2009). We have used 1 h resolution instantaneous ZTD post-processed values (GNSS precise orbits). The GNSS station at Granada (Granada station, EUREF code 13459M002), managed by the Instituto Andaluz de Geofísica, is equipped with a LEICA GRX1200PRO receptor. Only GNSS ultra-rapid orbits PWV data are available at Granada for the time period studied in this paper.

AMTD
8, 11077–11138, 2015

4.3 Lunar irradiance model

Barreto et al. (2013a) described that in lunar photometry it is necessary to use a lunar irradiance model to compute the Moon's extraterrestrial irradiance (I_0, Eq. 4 of Barreto et al., 2013a), to predict the changes in this quantity through the night. The Robotic Lunar Observatory (ROLO) at the United States Geological Survey (USGS) in Flagstaff, Arizona, has developed a model for the lunar spectral irradiance (Kieffer and Stone, 2005) as part of a NASA-funded effort for on-orbit calibration of remote sensing satellite instruments. The ROLO model can provide the exo-atmospheric lunar irradiance for any given location and time within its valid geometry range, and for any instrument's spectral response within its valid wavelength range. The model is based on fitting thousands of lunar measurements acquired over more than eight years with the ground-based ROLO telescopes in 32 wavelength bands from 350 to 2450 nm. Kieffer and Stone (2005) found band-averaged residuals $\sim 1\,\%$ from fitting the ROLO dataset with a function of only the geometric variables of phase angle and the sub-solar and sub-observer points on the Moon, i.e. the lunar librations. This value is a measure of the precision of ROLO model predictions of the lunar irradiance over its full range of geometries. For a given night of lunar photometer measurements, the relative prediction precision is well below 1 %. In this study, ROLO model computations of I_0 were provided by the USGS team as part of their support to AERONET.

5 Aerosols and PWV determination using the new CE318-T

5.1 Instrument's calibration

Similarly to the standard CE318-AERONET calibration, the CE318-T calibration during daytime period can be performed applying the standard Langley-Bouguer calibration at high mountain stations, using an integrating sphere for sky radiances calibration, or by

AMTD
8, 11077–11138, 2015

means of a cross-calibration transference technique. These methods are extensively described in Holben et al. (1998).

According to Barreto et al. (2013a), calibration under nighttime conditions can be also attained by transference from a calibrated instrument (using the ratio of moon measurements, hereinafter called Moon Ratio technique or $\mathrm{Ratio}_{\mathrm{moon}}$) but the absolute calibration can not be performed using the Langley-Bouguer technique. The reason is that, unlike the sun, the moon is a highly variable source which changes continuously with the lunar viewing geometry. Thus, Barreto et al. (2013a) developed the Lunar Langley Method modifying the usual Langley technique to be applied under variable illumination conditions, avoiding the determination of the instrument calibration every night. In this method the calibration coefficient for the instrument i (master with the superscript "M" or secondary with the superscript "S") can be expressed as,

$$V^i_{0,\lambda} = I_{0,\lambda} \cdot \kappa^i_\lambda \quad (1)$$

where $I_{0,\lambda}$ is the extraterrestrial irradiance in a certain channel with a central wavelength at λ, and κ^i_λ is the instrument's calibration constant, which depends on the instrument features. $I_{0,\lambda}$ is calculated using the ROLO model (Kieffer and Stone, 2005). κ_λ constant strictly accounts for the instrument's photometric responsivity and any residual systematic offset difference between ROLO predicted $I_{0,\lambda}$ and the real exoatmospheric irradiance.

Regarding the cross-calibration, and taking the advantage of the increased digital resolution and the simplicity that supposes the use of fixed internal gains, it is possible to establish a new way to transfer the moon absolute calibrations from a CE318-T master to an uncalibrated secondary CE318-T instrument using only daylight period measurements. In this case, we can consider similar the ratio master-secondary of averaged coincident raw data (digital counts or DCs) measured at daytime ($\overline{\mathrm{DC}^i_\mathrm{D}}$) and

AMTD
8, 11077–11138, 2015

at nighttime ($\overline{\mathrm{DC}^i_\mathrm{N}}$). Therefore,

$$V^\mathrm{S}_{0,\lambda} = V^\mathrm{M}_{0,\lambda} \cdot \frac{\overline{\mathrm{DC}^\mathrm{S}_\mathrm{N}}}{\overline{\mathrm{DC}^\mathrm{M}_\mathrm{N}}} \sim V^\mathrm{M}_{0,\lambda} \cdot \frac{\overline{\mathrm{DC}^\mathrm{S}_\mathrm{D}}}{\overline{\mathrm{DC}^\mathrm{M}_\mathrm{D}}} \tag{2}$$

with $\frac{\overline{\mathrm{DC}^\mathrm{S}_\mathrm{D}}}{\overline{\mathrm{DC}^\mathrm{M}_\mathrm{D}}} = \mathrm{Ratio}_\mathrm{sun}$. This new method avoids the use of nocturnal coincident measurements between master and secondary (or $\mathrm{Ratio}_\mathrm{moon}$), which are affected by higher uncertainties and have to meet restrictive criteria about moon illumination. Thus, the called Sun Ratio transference calibration makes the calibration of CE318-T instruments simpler and easier. It implies that, combining Eqs. (1) and (2), once a master instrument is moon calibrated using the Lunar Langley Method ($\kappa^\mathrm{M}_\lambda$) it is possible to find the spectral calibration constants for the secondary ($\kappa^\mathrm{S}_\lambda$) by means of coincident daytime measurements:

$$\kappa^\mathrm{S}_\lambda = \kappa^\mathrm{M}_\lambda \cdot \mathrm{Ratio}_{\mathrm{Sun},\lambda} \tag{3}$$

Implicit in this assumption is the fact that the lunar irradiance model ($I_{0,\lambda}$) is the same for master and secondary coincident measurements and also the fact that the $\mathrm{Ratio}_\mathrm{moon}$ and the $\mathrm{Ratio}_\mathrm{sun}$ are very close, which, in turn, depends on the value of the fixed resistance gains installed in each instrument. These resistances link detector voltages and output voltages, with a different configuration (in parallel or in series) depending on the type of measurement (sun mode or moon/sky mode). As a result, the goodness of the Eq. (3) depends on how uncertain is the assigned value of these resistances (∼ 1 %, given by the manufacturer), and the variability of these values between different instruments.

AMTD
8, 11077–11138, 2015

5.2 AOD and AE determination

Once κ_λ's are known, it is possible to determine instantaneous AOD from each individual measurement:

$$\mathrm{AOD}_\lambda = \frac{\ln(\kappa_\lambda) - \ln(\frac{V_\lambda}{I_{0,\lambda}}) - m_{\mathrm{atm}}(\theta) \cdot \tau_{\mathrm{atm},\lambda}}{m_{\mathrm{a}}(\theta)} \quad (4)$$

The subscript "atm" accounts for air mass and optical depth of all atmospheric attenuators with the exception of aerosols. This term includes the contribution of Rayleigh, O_3 and NO_2 optical depths, calculated using the same equations and resources as AERONET version 2. Atmospheric pressure has been estimated using the common hydrostatic equation because the information from the CE318-T integrated barometer was not available for the time period used in this study.

Since AE is a measure of the wavelength dependence of the AOD (Angström, 1929), it is a qualitative indicator of aerosol particle size (Kaufman et al., 1994) and useful to discriminate different atmospheric aerosol types. This parameter is usually retrieved using AOD within the spectral range between 870 and 440 nm. We can obtain AE using the following equation:

$$\ln(\mathrm{AOD}(\lambda_j)) = \ln(\beta) - \mathrm{AE} \cdot \ln(\lambda_j) \quad (5)$$

5.3 PWV determination

The Beer-Lambert-Bouguer Law must be modified in those spectral regions affected by strong spectral variation of molecular absorption. We do this taking into account the water vapor transmittance: $T_{\mathrm{w},\lambda}$ (Schmid et al., 1996). As Bruegge et al. (1992) and Halthore et al. (1997) showed, $T_{\mathrm{w},\lambda}$ present a exponential dependence with PWV:

$$T_{\mathrm{w},\lambda} = \exp(-a(m_{\mathrm{w}}(\theta) \cdot \mathrm{PWV})^b) \quad (6)$$

As shown by Barreto et al. (2013b) for nighttime period, the "a" and "b" constants can be determined by fitting the simulated $T_{w,\lambda}$ by a radiative transfer model for a specific filter function versus the PWV. Hence, PWV is obtained using the following expression:

$$\mathrm{PWV} = \frac{1}{m_w} \cdot \{\frac{1}{a} \cdot [\ln(\frac{I_{0,\lambda}}{V_\lambda}) + \ln(\kappa_\lambda) - m_R \cdot \tau_{R,\lambda} - m_a \cdot \mathrm{AOD}_\lambda]\}^{\frac{1}{b}} \quad (7)$$

In this equation, m_w represents the water vapor optical mass, m_R is the Rayleigh optical mass and $\tau_{R,\lambda}$ is the Rayleigh optical depth within water vapor absorption band. All these values have been obtained using AERONET version 2 references. $I_{0,\lambda}$ is obtained from the ROLO lunar irradiance model, AOD in this spectral region is obtained by extrapolation of AOD at 870 and 440 nm, and "a" and "b" constants are obtained by simulation of water vapor transmittances using the radiative code MODTRAN 4.0 (Berk et al., 1999) ($a = 0.732$ and $b = 0.611$).

6 AOD combined standard uncertainty estimation

In order to perform a quantitative estimation of the uncertainty involved in AOD retrieved by the CE318-T, we have followed the uncertainty propagation procedure described by the Joint Commitee for Guides in Metrology (JCGM, 2008). Equation (8) shows the estimated combined standard uncertainty in AOD (u_{AOD}) considering that the inputs (V_0, V and m) are not correlated. It is calculated using summation in quadrature of each term u_{xi}, which represents the standard uncertainty associated with each input. For the sake of brevity wavelength dependence on these inputs has not been included.

$$u_{AOD} = \sqrt{\frac{1}{m^2} \cdot \left[\left(\frac{\delta \mathrm{AOD}}{\delta V_0}\right)^2 \cdot u^2(V_0) + \left(\frac{\delta \mathrm{AOD}}{\delta V}\right)^2 \cdot u^2(V) + \left(\frac{\delta \mathrm{AOD}}{\delta m}\right)^2 \cdot u^2(m)\right]} \quad (8)$$

For daytime period we can consider negligible the instrumental uncertainty due to electro-optical precision (Holben et al., 1998) and due to airmass calculation. Consequently the uncertainty associated with the calibration term $u(V_0)$ is much larger than the uncertainty associated with the other terms. As a result we can estimate the uncertainty in AOD during daytime (u^{D}_{AOD}) as a function of the error of the zero airmass term modulated by the air mass:

$$u^{D}_{AOD} = \frac{1}{m} \cdot \frac{u(V_0)}{V_0} \tag{9}$$

As Holben et al. (1998) and Eck et al. (1999) suggested, the combined standard uncertainty of atmosphere, instrument noise and calibration in CE318-AERONET instruments can be inferred by means of the coefficient of variation (CV) of several V_0 values obtained at a reference station such as Mauna Loa. They found relative uncertainties for reference instruments better than 0.2–0.5 and ∼ 1.5 % for field instruments in the visible and the near infrared (IR) range (Eck et al., 1999; Schmid et al., 1999). This yields an uncertainty due to calibration ($u(V_0)$) between 0.002 and 0.005 for reference instruments and ∼ 0.015 for instruments calibrated by means of intercomparison techniques. Following Eck et al. (1999) and Toledano et al. (2007), it is necessary to include the errors associated with the estimation of Rayleigh optical depth and gaseous absorptions. In case of CE318-T at daytime period, we also expect negligible instrument uncertainty $u(V)$ (since dark current and triplets are considerably low) as well as similar estimations for Rayleigh and gases optical depths. Assuming the values proposed by Eck et al. (1999), a total AOD uncertainty (u^{D}_{AOD}) of ∼ 0.002–0.009 is estimated for reference instruments, and ∼ 0.010–0.021 for field instruments. Daytime calibration uncertainty due to Langley and intercomparison procedures are also expected to be similar for CE318-T and CE318-AERONET. These assumptions will be discussed in Sect. 6.1.

In case of nighttime measurements, taking into account Eq. (1), an alternative form of Eq. (8) is required, including three additional terms. Two terms attributed to the contribution of $u(V)$ and the uncertainty in the ROLO model ($u(I_0)$), and another term which includes the correlation coefficient r (often called covariance term) of the correlated inputs κ and I_0 (Eq. 10). Please note that the term $u(\kappa)$ corresponds to the uncertainty

Discussion Paper | Discussion Paper | Discussion Paper | Discussion Paper |

AMTD
8, 11077–11138, 2015

The new sun-sky-lunar Cimel CE318-T multiband photometer

A. Barreto et al.

due to calibration, and it is similar to the calibration term involved in Eq. (9) for daytime measurements ($u(V_0)$ in this case).

$$
\begin{aligned}
{u^{\mathrm{N}}_{\mathrm{AOD}}}^2 &= \frac{1}{m^2}\left(\frac{u^2(\kappa)}{\kappa^2} + \frac{u^2(I_0)}{I_0^2} + \frac{u^2(V)}{V^2}\right) + \\
&+ \frac{2}{m^2}\cdot r_{\kappa,I_0}\cdot\left(\frac{\delta\mathrm{AOD}}{\delta\kappa}\right)\cdot\left(\frac{\delta\mathrm{AOD}}{\delta I_0}\right)\cdot u(\kappa)\cdot u(I_0) \\
&\sim \frac{1}{m^2}\left(\frac{u^2(\kappa)}{\kappa^2} + \frac{u^2(I_0)}{I_0^2} + \frac{u^2(V)}{V^2}\right)
\end{aligned}
\qquad (10)
$$

Although the existence of a correlation between κ and I_0 can be anticipated, the covariance term is expected to be near 0. The reason for neglecting this term is the low impact of I_0 systematic uncertainties on κ during the Langley period (≤ 2 h). In any case, considering these two magnitudes are inversely correlated (negative covariance), by neglecting this term we are obtaining a conservative estimate of the total uncertainty for the nighttime period. Equation (10) presents a combined uncertainty in AOD measurements at nighttime related to the random uncertainties in calibration process as a result of the linear regression analysis ($u(\kappa)$) in addition to the systematic uncertainties due to ROLO estimations ($u(I_0)$) and instrument uncertainty ($u(V)$). Kieffer and Stone (2005) estimated a relative accuracy of this model ≤ 1 %, and therefore we expect an additional error in computed AOD of ≤ 0.01. The term in Eq. (10) associated with the instrument calibration can be obtained, similarly to daytime period, by means of CVs of the κs obtained from Lunar Langley-calibrated instruments. The estimate of calibration uncertainty at nighttime for field instruments can be performed by analyzing the difference between sun and moon ratios in case of instruments calibrated using Moon Ratio technique. An additional error in AOD determination must be included when the Sun Ratio technique is applied. This term is dependent on the precision in the measurement of the internal resistance gains which relate the sun and moon/sky scenarios and therefore the $\mathrm{Ratio_{sun}}$ and the $\mathrm{Ratio_{moon}}$ values. We will estimate and discuss these nocturnal instrument calibration uncertainties for field instruments in Sect. 6.2. The last term in Eq. (10) represents the uncertainty due to instrument precision. This term will be determined in Sect. 6.1 using of the normalized range of three consecutive measurements (triplets), in the same way that normalized standard deviations or CVs are used to determine $u(\kappa)$). In our case, since we are working with a set of data with just three measurements, normalized range and normalized standard deviation of triplets are similar quantities. We have empirically determined they differ in a factor of two (normalized range are ~ two times the normalized standard deviation).

Finally, it is important to highlight that these errors are modulated by the air-mass term, and therefore all these expected values are the maximum AOD errors at $m = 1$ (for solar noon and highest moon elevation conditions), and are reduced by a factor of $1/m$ as the zenith angle becomes higher, with a minimum at sunset and sunrise at daytime, and at moonrise and moonset at nighttime.

6.1 u_{AOD} estimation for reference instruments

Firstly, we have estimated the uncertainty in calibration for reference instruments (Langley calibrated). To do this, we computed at IZO the spectral calibration coefficients $V_{0,\lambda}$ for daytime and the calibration constant κ_λ for nighttime for the CE318-T master using the Langley-Bouguer technique and the Lunar Langley Method from the average of 20 days (from February to May 2014) and 6 nights (March to June 2014), respectively. These days and nights were affected by low and quite stable aerosol loads. CV for daytime Langley calibration is ≤ 0.31 %, similar to those presented in Holben et al. (1998) for Mauna Loa reference sunphotometers. It demonstrates that we can consider the same calibration uncertainty for CE318-T and CE318-AERONET Langley-calibrated instruments during daytime, as suggested previously. For nighttime, CVs range from 0.39 to 0.78 % for visible channels, to values of 0.73 and 1.24 % for 1020 and 1640 nm, respectively. It leads to an uncertainty calibration estimation of 0.004–0.008 for visible channels and 0.007–0.014 for near-IR channels in case of reference instruments. Ac-

AMTD
8, 11077–11138, 2015

cording to Eq. (10), a value of 0.01 must be added due to uncertainties in the ROLO irradiance model and also a value of $u(V)$ as a result of instrumental uncertainties.

Secondly, a comparison analysis on the triplets measured by two masters installed at IZO, the CE318-T and the CE318-AERONET, has been performed in order to check the performance of the new CE318-T tracking system as well as to estimate the instrument precision term ($u(V)$) in Eq. (10). For this study AERONET level 1.5 triplets have been used. Only very stable aerosol conditions have been chosen to analyze triplets variability, selecting a set of 23 days (between February and March 2015) characterized by low AOD at 500 nm values (≤ 0.02). We can see in Fig. 1a significantly lower triplet variability values at all wavelengths for CE318-T compared to the previous CE318-AERONET. The higher variability in CE318-AERONET 1020 nm channel indicates a possible problem affecting this channel, in addition to the expected uncertainties due to the lack of temperature correction in this level 1.5 data version. The rest of channels showed CE318-T mean triplets values between 112 and 172 % lower than those values for CE318-AERONET. It indicates the better performance of this new tracking system, pointing to an improved precision of CE318-T compared to previous sunphotometer versions. However, it is fair to admit that a final confirmation of the CE318-T precision improvement must be given after using data from several instruments.

We have also analyzed the variability of CE318-T triplets at nighttime, including a set of seven nights near full moon and five nights near quarter moon between January and April 2015 (Fig. 1b). Generally, triplets measured under near full moon conditions are lower than 0.2 %, similar to the CE318-AERONET daytime triplet values. For low illumination conditions triplets are higher, up to 1 % in all channels with the exception of 440 nm, with triplets up to 2 %. Thus, the additional uncertainty due to measurement errors is dependent on illumination conditions and is half of the triplets normalized range (an estimation of the normalized standard deviation), with a value ≤ 0.001 for near full moon and 0.005 for near quarter moon (0.01 in case of 440 nm channel). With this information we can estimated the combined AOD standard uncertainty at nighttime for a reference instrument is 0.011–0.013 (0.012–0.014) in case of visible channels

AMTD
8, 11077–11138, 2015

and full moon (quarter moon) conditions, with values up to 0.016 in 440 nm channel at higher phase angles. For near-IR wavelengths we have obtained a combined standard uncertainty estimation in AOD ranging from 0.012 to 0.017 for full moon conditions and between 0.013 and 0.018 for quarter moon.

6.2 u_{AOD} estimation for field instruments

In order to estimate the combined standard uncertainty in AOD measurements for CE318-T field instruments we performed the calibration of a secondary instrument using coincident master/secondary measurements taken under stable atmospheric conditions in 22 consecutive days (from 9 to 30 June 2014) and 10 consecutive nights (from 9 to 20 June 2014) in order to ensure the validity of Eq. (3) for $\kappa_{\lambda}^{\mathrm{S}}$ estimation. The different spectral ratio in this lunar cycle at each channel was calculated to show the ratio variability at daytime and nighttime conditions throughout the lunar cycle (Fig. 2 for 11 consecutive days and 10 consecutive nights). We observe that the ratio of measurements during day and night are quite similar in case of high moon illumination conditions, and the ratio performed using nocturnal measurements presents higher dispersion with decreasing moon's illumination. We have found similar standard deviations (σ's) at daytime and at nighttime for ±1 night around full moon conditions and ratio sun/moon relative differences (Δratio) $< 0.3\,\%$ for visible channels (see information included in this figure). Higher Δratio values were obtained for 1020 nm channel (0.57 %), attributed to the temperature effect at this spectral range. It implies that a new uncertainty term must be assumed for instruments calibrated by means of the Moon Ratio technique (0.006 for 1020 nm channel and 0.003 for the rest of channels). Consequently, following Eq. (10), a CE318-T instrument calibrated by means of the Moon Ratio calibration technique has a combined standard estimated uncertainty for visible channels of 0.011–0.013 (0.012–0.014) under full moon (quarter moon) conditions, with the exception of 440 nm channel at higher phase angles, with values up to 0.017. In 1640 nm range, we have obtained uncertainties ranging from 0.013 to 0.017 (0.014

Discussion Paper | Discussion Paper | Discussion Paper | Discussion Paper |

AMTD

8, 11077–11138, 2015

The new sun-sky-lunar Cimel CE318-T multiband photometer

A. Barreto et al.

to 0.018) for full moon (quarter moon), and for 1020 nm channel these values range within 0.014–0.018 (0.015–0.019) for full moon (quarter moon).

In case of field instruments calibrated by means of the Sun Ratio technique we have to take into account the present precision ≤ 1 % in the instrumental resistance gains given by the manufacturer. In this respect we have studied the difference between $Ratio_{sun}$ and $Ratio_{moon}$ in near full moon events for seven different heads (all of them installed at IZO during 2014). Our results showed this relative difference is within the ±1 % stated by the manufacturer as the precision limit, wavelength dependent (Fig. 3). Indeed, this figure shows relative differences < 0.5 % for $\lambda \leq 870$ nm and values up to 0.8 % for near-IR channels. With this information the additional uncertainty term in those instruments Sun Ratio calibrated can be fixed to values ≤ 0.8 % for near-IR channels and ≤ 0.5 % for channels in the visible range. Therefore, following Eq. (10), the combined nocturnal AOD uncertainty due to κ, I_0 and V uncertainties in a Sun Ratio calibrated field instrument is expected to be from 0.012 to 0.014 (0.013 to 0.015) for visible wavelength channels at full (quarter) moon conditions with the exception of 440 nm, with values up to 0.017 in case of low moon illumination. For near-IR channels we obtained values from 0.015 to 0.019 (0.016 to 0.020) for 1640 nm channel under full (quarter) moon events, and between 0.016 and 0.020 (0.017 and 0.021) in the case of 1020 nm channel. It assures the validity of the Sun Ratio method for CE318-T calibration as a simple technique with relatively low uncertainties (maximum uncertainties expected to be ≤ 0.021), reducing considerably the complexities of the former Moon Ratio technique.

6.3 Case study to estimate CE318-T precision

Precision, defined as the capability of the instrument to perform measurements repeatably and reliably, can be inferred from the information extracted from the triplets, as we did previously in Sect. 6.1. However, it is also possible to determine the precision in AOD through an analysis of the AOD measurements and their dispersion under very stable AOD conditions. Thus, the standard deviation in AOD (σ(AOD)) in such condi-

AMTD
8, 11077–11138, 2015

tions provides the information about instrument's precision. For this purpose, we have selected a case study at IZO of three different days and nights between 15 and 18 March 2014, in which AOD conditions were quite stable and moon's illumination was high (full moon in 16 March). In fact, these conditions will be used in Sect. 8 to study into detail the CE318-T performance. We have coincident daytime AOD information in this time period from the CE318-T master, the CE318-AERONET master and the PFR, as well as nighttime AOD information from the same CE318-T master.

Averaged AOD values at daytime of 0.019, 0.013 and 0.013 were found for PFR, CE318-AERONET and CE318-T, respectively, confirming the low aerosol loads in this period. Nighttime averaged AOD was 0.022. The stable AOD conditions were confirmed by means of the analysis of the σ(AOD) of each instrument, with daytime values of 0.009, 0.004 and 0.003 for PFR, CE318-AERONET and CE318-T, respectively, and nighttime values of 0.003. These results confirmed that the CE318-T precision is similar to other reference instruments for both daytime and nighttime (under near full moon conditions).

7 CE318-T intercomparison with reference instruments

The CE318-T AOD and PWV characterization and assessment was carried out at IZO and Granada. Daytime observations at IZO encompass daytime measurements in 2014 taken in 60 days from 1 March to 30 June, meanwhile at nighttime the study is focused on 32 nights, corresponding to four different moon cycles in 2014: 12–23 March, 7–19 April, 7–13 May and 9–16 June. Nocturnal evaluation performed at Granada station involves four nights of collocated measurements CE318-T/star-photometer on 7–8, 9–10, 11–12 and 14–15 August 2014.

Discussion Paper | Discussion Paper | Discussion Paper | Discussion Paper |

AMTD
8, 11077–11138, 2015

7.1 Assessment of the Sun Ratio calibration method

In order to confirm the suitability of the nocturnal calibration transference using the Ratio Sun technique, we have computed the scatterplot of AOD coincident measurements performed at IZO by the master (direct sun and moon calibrated using the Langley and the Lunar Langley methods according to Sect. 6.1), and the secondary (sun calibrated using calibration transference and moon calibrated using both the Sun Ratio and Moon Ratio techniques) (see Fig. 4). The main statistics of the comparison are presented in Table 1. We observed a good agreement between the AOD retrieved at daytime from the master and the secondary (MB and RMSE values ≤ 0.002). For nighttime we obtained similar results by calibrating the secondary instrument using the $\mathrm{Ratio}_{\mathrm{sun}}$ or the $\mathrm{Ratio}_{\mathrm{moon}}$, with MBs and RMSEs slightly higher using daytime ratios, but in all cases within the expected precision for a reference instrument (MBs < 0.004 and RMSEs < 0.008).

7.2 AOD daytime period intercomparison at IZO

We have used three independent and collocated measurements at IZO from PFR, PSR and CE318-AERONET to validate the master CE318-T performance during daytime. As WMO (2005) stated, the preferred method of traceability to evaluate the instrument's accuracy is by means of co-location of representative networks instruments performed at reference wavelengths, trying to ensure a minimum wavelength difference between their channels. Since CE318-T and PFR take measurements at different wavelengths, it is not possible to perform such comparison at all CE318-T channels. For this reason, we have selected for this intercomparison the channels centered ~ at 870 and 500 nm.

There are other specific limits established by WMO (2005) to ensure successful comparisons, besides the minimum wavelength criteria. These limits are: (1) more than 1000 coincident points, (2) minimum of five clear sky days, and (3) AOD values within 0.040–0.200 range during the comparison period. In this study we have satisfied all

Discussion Paper | Discussion Paper | Discussion Paper | Discussion Paper |

AMTD

8, 11077–11138, 2015

The new sun-sky-lunar Cimel CE318-T multiband photometer

A. Barreto et al.

Title Page
Abstract Introduction
Conclusions References
Tables Figures
◂ ▸
Back Close
Full Screen / Esc
Printer-friendly Version
Interactive Discussion

the aforementioned limits, as can be seen in the text included in Fig. 5, where the main results of the intercomparison are shown.

In a first stage, we have compared quasi-coincident (±1 min) AOD measurements at daytime period extracted from CE318-T and CE318-AERONET in the 60 days period from March to June 2014 (Fig. 5). MB ≤ 0.001 and RMSE ≤ 0.002 were obtained, in addition to high regression coefficients > 0.99. These values are consistent with the AOD uncertainty associated with high mountain calibrated reference instruments presented by Eck et al. (1999).

A subsequent intercomparison study using CE318-T and PFR, as well as between CE318-T and PSR in the same period encompasses coincident daylight measurements at IZO in a temporal window of ±1 min. We can see a good agreement between AOD extracted from CE318-T and PFR/PSR instruments ($r > 0.99$) and MBs and RMSEs below 0.003 for PFR, and MBs and RMSEs below 0.006 for PSR. Skill scores obtained for CE318-T and PFR are similar to the values obtained by Nyeki et al. (2013) in a five-month comparison at IZO in 2009 and better than those found by Kazadzis et al. (2014) in Athens, Greece, using ground instruments. We have also compared collocated PSR/PFR, AERONET/PFR and AERONET/PSR, finding similar results to those obtained in the two last comparisons (MBs ≤ 0.003 and RMSEs ≤ 0.006 for all comparisons in both channels).

WMO (2005) also stated that an acceptable traceability exists only if differences in AOD between reference instrument lie within acceptance limits, which are defined for finite field of view (fov) instruments in function of airmass (m_a). They defined the expanded uncertainty limits at a 95 % of confidence level as $U_{95} = \pm(0.005+0.010/m_a)$, matching the two standard deviation level for a Gaussian distribution. Therefore, this type of criterion assumes that our error distribution follow a normal distribution. All the U_{95} values for all instruments in this comparison are within the specified limits (Fig. 6). U_{95} levels are similar to the values obtained by Nyeki et al. (2013) when comparing the standard CE318-AERONET with PFR at IZO. Values for 870 nm channels they are

AMTD
8, 11077–11138, 2015

also in agreement with those results found by Kazadzis et al. (2014) for AERONET-PFR comparison at Athens, but our results for 500 nm channel are considerably better.

Consequently, we have obtained similar AOD differences at daytime between CE318-T and reference instruments, as the current CE318-AERONET master and the PFR. As a result we can anticipate a precision of the new CE318-T at daytime similar to the other reference instruments, which is in agreement with the expected daytime accuracies presented in Sect. 6.

7.3 AOD nocturnal intercomparison at Granada

Coincident measurements of the CE318-T secondary instrument (Sun Ratio calibrated) and the star photometer in a temporal window of ±15 min were performed at Granada during four nights in August 2014 (7–8, 8–9, 11–12 and 14–15). During this period, stellar information in 880, 500 and 440 nm channels, close to CE318-T wavelengths, were extracted. Main statistics of the comparison are presented in Table 2, showing high regression coefficients for the three channels and reduced MBs and RMSEs values in case of longer wavelength channels (≤ 0.001 for 870 nm and ≤ 0.013 for 500 nm). Higher discrepancies were found in the case of 440 nm channel (MB = -0.033 and RMSE = 0.018). The sequence of AOD measured at 500 nm by CE318-T at day and nighttime are displayed in Fig. 7 as well as star photometer nighttime AODs. The scatterplot of AOD extracted from these two instruments at 870, 500 and 440 nm channels is shown in Fig. 8. There is a good agreement between both instruments in the case of 870 and 500 nm channels, with discrepancies lower than the expected accuracies for the star photometer published by Pérez-Ramírez et al. (2011) and also lower than the errors presented in Sect. 6 for field instruments. On the contrary, the differences found in the case of 440 nm channel are higher than those expected for star photometry and slightly higher than the maximum uncertainty values for CE318-T field instruments in visible channels theoretically estimated using Eq. (10) (≤ 0.017 for secondary Sun Ratio calibrated instruments). This might be attributed to a calibration problem in the star photometer in this channel.

AMTD
8, 11077–11138, 2015

7.4 AOD day/night transition coherence test

The daytime and nighttime AOD evolution extracted at IZO from the CE318-AERONET master and the CE318-T master for a sequence of four moon cycles in March, April, May and June 2014 (60 days and 32 nights) is shown in Fig. 9. The moon's fraction of illumination (FI) is also depicted in each AOD figure to show the accuracy dependence of CE318-T nocturnal retrievals with the lunar phase. An artificial AOD cycle with moon's zenith angle is readily observed in Fig. 9 for case of low AOD events. The result is a curvature in AOD with maximum absolute values when the moon zenith angle is minimum. This cycle is more important in case of 1640 nm channel. The quantitative analysis of AOD differences between daytime and nighttime period with respect to FI are shown in Tables 3 and 4, in which we have compared nocturnal (CE318-T) and daytime (CE318-AERONET) data corresponding to the consecutive 1-h time period during moonset-sunrise (MS-SR, 23 events) and sunset-moonrise (SS-MR, 20 events) for different illumination conditions, assuming stable AOD conditions. In this respect, no significant changes in aerosol loads were observed during this period, with the exception of the variations in AOD observed on 10–11 May and on 12–13, 14–15 and 15–16 June. These data have not been included in the analysis. MS-SR events are representative of conditions before full moon while SS-MR events are typically observed after full moon. These tables show that, in general for MS-SR events, MBs for shorter wavelengths channels ($\lambda \leq 870$ nm) and for any illumination condition are ≤ 0.015, slightly higher than the values reported by Eck et al. (1999) and Schmid et al. (1999) for reference instruments but within the expected uncertainties calculated in Sect. 6. Somewhat higher differences appeared in SS-MR events, when MBs and RMSEs ≤ 0.018 (0.022 for 440 nm channel) are retrieved, with the exception found at FI between 70 and 80 %, when we obtained a MB of 0.024 for 870 nm channel, while a MB value of −0.001 is obtained for similar illumination conditions in case of MS-SR period. In case of longer wavelength channels (1020 and 1640 nm) we have found significant discrepancies for low illumination conditions (MBs > 0.06), especially in 1640 nm channel, with higher dif-

AMTD
8, 11077–11138, 2015

ferences after full moon conditions. In these channels MBs < 0.02 can only be found under FI $\geq 90\,\%$. Generally, the lower RMSE values the higher moon's illumination.

This information shows that the values estimated by Eq. (10) and presented in Sect. 6 for CE318-T nocturnal AOD uncertainty match reasonably well the mean differences obtained in this coherence test for visible channels under all illumination conditions (up to 0.016 for reference instruments) and for near infrared channels (up to 0.018 for reference instruments) only for high FI conditions ($> 90\,\%$). The artificial nocturnal cycle on AOD is observed for any wavelength, with a minor impact at $\lambda < 1020$ nm, being the channel centered at 1640 nm the most affected channel. The reason for this nocturnal cycle is unclear, and further investigations must be developed to clarify it, although it possibly reflects a problem in the instrument calibration, in the nighttime AOD calculation and/or in the lunar irradiance model.

7.5 Precipitable Water Vapor intercomparison

We have compared ±15 min quasi-coincident daytime PWV data from the master CE318-T with CE318-AERONET data (Fig. 10a) and GNSS precise orbits for daytime and nighttime at IZO (Fig. 10b). In the same time period as in previous sections, PWV measured with GNSS was 0.37 and 0.32 cm during daytime and nighttime, respectively, and 0.29 cm for both daytime and nighttime in case of CE318-T. We have used the same criteria as in the previous AOD comparison to determine quantitatively the nocturnal discrepancies as a function of FI. This information is presented in Table 5. Daytime CE318-T PWV matches reasonably well AERONET data, with discrepancies and RMSEs ~ 0.02 cm and high regression coefficient ($r = 0.99$). The daytime comparison of CE318-T against GNSS data (Fig. 10b) also showed a good correlation between data ($r = 0.97$) but higher MBs (−0.09 cm), showing the existence of a slight negative bias between instruments, and slightly higher RMSEs (0.05 cm). In case of nocturnal data, we observe a similar negative bias to those obtained at daytime. MB values remain lower than daytime values for any FI. Regarding RMSE, only near full moon events have similar RMSEs than daytime period. We obtained RMSE values ranging from 0.09 cm for FI < 60% to 0.05 cm under near full moon events. Daytime as well as nocturnal measurements are within the expected precision of CE318-AERONET and GNSS under such dry conditions, as reported by Schneider et al. (2010). These authors found a CE318-AERONET expected precision ranging from 7 to 25 %, from dry to humid conditions, the GNSS precision was within 10–20 %, in case of PWV $\leq$ 0.35 cm, as in our case. These values also agree with the values found by Barreto et al. (2013b) in the comparison between CE318-U and GNSS PWV data.

PWV comparison at Granada allows us to extend the last evaluation procedure to wetter conditions, including GNSS data for nine different days and five different nights in August 2014 (Fig. 10c), with PWV values up to 3 cm. The comparison criteria is also ±15 min. Since this information has been obtained using the secondary CE318-T instrument, it has served us as a new evaluation of the secondary's calibration. PWV averaged during this period is 1.70 cm for GNSS and 1.55 cm for CE318-T for daytime, and 1.90 and 1.98 cm, respectively, for nighttime. We have found MBs of −0.15 and 0.09 cm, for daytime and nighttime, respectively, both within the 7–25 % precision expected for CE318-AERONET and 10–20 % precision for GNSS. RMSEs of 0.14 and 0.07 cm and regression coefficients of 0.83 and 0.85 were obtained, respectively.

8 Demonstration case study

The purpose of these case studies is to assess in more detail the performance of the master CE318-T under both very clean free troposphere and dusty conditions, with a quick transition between the two scenarios. This case analysis also provides an opportunity to explore new potential scientific applications of CE318-T since it can measure diurnal changes of aerosols and water vapor (during daytime and nighttime periods) with high temporal resolution, helping to improve our understanding on short-term atmospheric processes.

AMTD
8, 11077–11138, 2015

8.1 IZO, June 2014

During the period 10–18 June 2014 three dust laden intrusions of the SAL, followed by clean background free troposphere conditions, were recorded at IZO with the MPL and the CE318-T (Fig. 11). The coherence between the backscatter signal (Fig. 11a) and the AOD evolution (Fig. 11b) can be seen in this figure. The onset of two of the three dust intrusions are clearly detected in both figures in the late hours of 12 June and also in the first hours of 15 June. The intrusion detected by CE318-T on 14 June was not recorded by MPL because the presence of thick clouds observed at altitudes below IZO, which completely attenuated the lidar signal. Regarding the AE evolution (Fig. 11c) we observe a good agreement between daytime and nighttime measurements during SAL conditions, as is the case of 13 June. However, we observe the presence of a diurnal cycle in AE under free troposphere conditions, with predominantly higher values of AE at nighttime. The first feature is a consequence of the homogeneity of SAL conditions in terms of aerosol properties (Smirnov et al., 1998), while the second feature is attributable to the strengthening of free-troposphere conditions driven by the katabatic regime during nighttime, causing an increase in AE associated with pristine near aerosol-free Rayleigh conditions. This figure also shows the expected higher dispersion in AE as moon's illumination drops. Other assessments can be done from the PWV records (Fig. 11d) within the three SAL events. The expected increase in PWV as a result of the dust intrusions is observed. Saharan air masses are characterized by relatively low and stable humidity levels but higher than those normally present under clean free troposphere conditions, driven by a subsidence regime. This is the case of 13 June at night and 14 June at noon, perfectly matching the dust intrusions. These features were similarly detected by GNSS.

8.2 IZO, March 2014

This is an example of free troposphere conditions affecting IZO during several days (Fig. 12). In this case, from 16 to 21 March, there existed pristine conditions, with AOD

AMTD
8, 11077–11138, 2015

below 0.05 (Fig. 12b). Even under these background conditions, data from the CE318-T reveals valuable information of atmospheric processes. A diurnal cycle in AE is still present, where the AE typically reaches its minimum approximately in the early hours of the morning, between 04:00 and 06:00 UTC, while the maximum is reached in the second half of the day (Fig. 12c). Regarding PWV, we have found that, under these free troposphere conditions, both CE318-T and GNSS are capable of detecting a diurnal variation in atmospheric humidity with maximum during daytime. The diurnal cycle is still an issue that is currently being investigated and some explanations have been hypothesized. Some authors have analyzed GNSS data partially and attribute the PWV diurnal variation to an artifact related with diurnal changes of the mean temperature of the layer (Ortiz de Galisteo et al., 2010). Other authors explain these variations by diurnal variations of temperature and winds (Suparta et al., 2009), water vapor transport by turbulent mixing with the development of the boundary layer in the afternoon (Wu et al., 2003) or by evaporation and condensation within the air mass and wet or dry advections by local winds (Ortiz de Galisteo et al., 2010). In our case, we attribute the PWV diurnal variation to diurnal evolution of the marine boundary layer which introduces small amounts of water vapor in the free troposphere near noon, reinforced by the sharp topography of the island and the consequent valley-land breeze system established on a daily basis. This is confirmed by the diurnal evolution of the boundary layer (BL) top altitude (not shown here) which can vary over 1000 m between noon and midnight. The BL top height has been obtained from radiosonde data at 00:00 and 12:00 UTC from the WMO GUAN station # 60018 (Güímar, Tenerife), 13 km distance from IZO. The criteria used to account for the BL top altitude are $\Delta\theta/\Delta z \geq 0.0025\,\mathrm{km}^{-1}$ and $\theta_{top}/\theta_{base} \geq 1\,\mathrm{K}$, where $\Delta\theta/\Delta z$ is the potential temperature lapse rate, and θ_{top} and θ_{base} correspond to the top and base of the layer, respectively (Cuesta et al., 2008; Guirado et al., 2014).

With this information we can verify that CE318-T has sufficient accuracy to capture the diurnal cycle of aerosols and PWV associated with local and short-term atmospheric variations. These examples show us the high sensitivity of the new CE318-T

AMTD
8, 11077–11138, 2015

photometer, capable of detecting small-scale atmospheric processes which will permit new studies which were impossible to tackle before with standard sun photometers.

9 Summary and conclusions

In this paper we have described the new photometer CE318-T, designed to perform a complete cycle of diurnal photometric measurements during both daytime and nighttime. New improvements permit this new photometer to extend photometric information at nighttime using the moon as a light source. Our comparative results of the instrument's triplets measured by two masters (CE318-T and CE318-AERONET) installed in IZO showed a better precision of the CE318-T as a result of its improved tracking system. We have also presented the methodology to calibrate the instrument absolutely (by means of the Langley and the Lunar Langley techniques, for day and night measurements, respectively), and by means of a calibration transference from a master (using the new Sun Ratio technique). The last technique allow us to reduce the complexities inherent to nocturnal calibration due to the low signal captured at nighttime. We assessed the Sun Ratio technique by an AOD intercomparison of a master CE318-T Langley-calibrated with a secondary instrument calibrated using this method. A good agreement between both AOD retrievals was found, with MB < 0.002 for daytime and < 0.004 for nighttime.

Our analysis, following the error propagation theory, resulted in a estimation of the combined CE318-T AOD standard uncertainty. For daylight period (u^{D}_{AOD}) we expect similar values to those calculated for previous sunphotometer versions, ranging between 0.002 and 0.009 for reference instruments and ~ 0.015 for field instruments. For nighttime period, we estimated u^{N}_{AOD} values for reference instruments of 0.011-0.014 for visible channels (with the exception of 440 nm, with values up to 0.016 for higher phase angles) and 0.012–0.018 for near-IR channels. For field instruments calibrated using the Moon Ratio technique we have estimated u^{N}_{AOD} between 0.011 and 0.019. If the new Sun Ratio technique is applied, higher uncertainties are expected: 0.012–

AMTD
8, 11077–11138, 2015

0.015 (0.017) for visible (440 nm) channels and 0.015–0.021 for longer wavelengths. To summarize, maximum uncertainties of 0.017 are expected in visible channels and 0.021 in the case of longer wavelengths, all of them for low moon's illumination conditions. These values are the maximum expected values for a typical air mass value of $m = 1$.

We derived daytime AOD for 60 days in March, April, May and June 2014, at IZO using a CE318-T reference instrument (Langley-calibrated). We compared these observations with those extracted from independent reference instruments (CE318-AERONET and PFR) and the PSR prototype, as an assessment of the instrument performance. This AOD comparative study at daytime reported discrepancies similar to sun photometry precision in the AERONET or GAW-PFR networks (≤ 0.01), also similar to the $u_{\text{AOD}}^{\text{D}}$ estimated values. The nocturnal evaluation performed in Granada station using a star photometer and a secondary CE318-T showed similar low discrepancies for 870 and 500 nm channels (~ 0.01), within the $u_{\text{AOD}}^{\text{N}}$ expected values, but higher (~ 0.03) for 440 nm channel. We attributed this discrepancy to a calibration problem in the star photometer in this channel.

A subsequent coherence test for AOD at IZO using the CE318-T and CE318-AERONET masters was focused on the AOD daytime and nighttime differences between 1 h after and before sunset and sunrise. The results of this coherence test match reasonably well the u^{N}AOD estimated values in case of visible channels at all illumination conditions. However, in case of near infrared channels, this consistency was only attained in high FI conditions ($> 90\,\%$). This test also reflects the existence of a faint nocturnal cycle on AOD which impacts more significantly in 1640 nm channel. This cycle possibly reflects a problem in instrument calibration, in nighttime AOD calculation or in the lunar irradiance model, and further investigations must be carried on to properly identify and quantify the causes of the problem.

Regarding PWV, the comparison showed a good agreement between PWV CE318-T/CE318-AERONET and CE318-T/GNSS obtained at day and nighttime conditions for any illumination condition. MB and RMSE values < 0.1 cm were found in case of dry

AMTD
8, 11077–11138, 2015

conditions, when the precision of water vapor measurements is low. We found also a slight negative bias between CE318-T and GNSS for daytime and nighttime.

The final part of this paper examines two cases studies at IZO in 2014, including a sequence of dust intrusions and clean free-troposphere events (in June) and a sequence of clean conditions representative of the free troposphere (in March). These two cases showed that the CE318-T has sufficient accuracy to capture the diurnal cycle of aerosols and PWV associated with local and short-term atmospheric variations, important for climate studies.

Though these results reveal a good performance of CE318-T in comparison to the current standard instruments, showing better precision in terms of instrument pointing, it is fair to admit that a definitive conclusion about CE318-T accuracy and precision must be stated after analyzing several instruments. Further investigations are needed to determine the uncertainty reduction that the use of the integrated pressure sensor might suppose instead of using the hydrostatic equation and the NCEP/NCAR Reanalysis. Furthermore it is necessary to conduct a comprehensive investigation of the ROLO model used in this paper to perform a conclusive estimation of the uncertainties involved in it.

The comparable daytime and nighttime measurements also permit to include nocturnal aerosol information in the existing databases. It is of crucial importance for monitoring aerosol transport, especially in high latitude locations, given the extended periods of darkness during winter, to study the effect of aerosol particles on cloud lifetime or nocturnal coverage, and for detecting the sharp changes that aerosol concentration may experience in term of hours during dust events.

To conclude, these results demonstrate the capability of the new CE318-T for aerosols and atmospheric water vapor monitoring although further investigations must be carry out to confirm them at different locations, in a wider range of moon's illumination and cycles and using different CE318-T photometers.

Acknowledgements. This work has been developed within the framework of the activities of the World Meteorological Organization (WMO) Commission for Instruments and Methods of Observations (CIMO) Izaña Testbed for Aerosols and Water Vapor Remote Sensing Instruments. The Granada GNSS station belongs to the Instituto Andaluz de Geofísica. The AERONET sun photometers at Izaña have been calibrated within the AERONET-Europe TNA, supported by the European Community-Research Infrastructure Action under the FP7 ACTRIS grant agreement no. 262254. The GAW-PFR network for AOD at WMO-GAW global observatories has been implemented by the World Optical Depth Research and Calibration Center (WORCC). This work has also been supported by the Andalusia Regional Government through projects P12-RNM-2409 and P10-RNM-6299, by the Spanish Ministry of Science and Technology through project CGL2013-45410-R; and finally by the EU through ACTRIS project (EU INFRA-2010-1.1.16-262254). The authors wish to thank to Ángel Gómez Peláez and Alberto Redondas to assist the authors in the instrument's uncertainty estimation.

References

Angström, A. K.: On the atmospheric transmission of sun radiation and on the dust in the air, Geogr. Ann.,12, 130–159, 1929. 11093

Ansmann, A., Wagner, F., Althausen, D., Müller, D., Herber, A., and Wandinger, U.: European pollution outbreaks during ACE 2: Lofted aerosol plumes observed with Raman lidar at the Portuguese coast, J. Geophys. Res., 106, 20725–20733, 2001. 11082

Baibakov, K., O'Neill, N. T., Ivanescu, L., Duck, T. J., Perro, C., Herber, A., Schulz, K.-H., and Schrems, O.: Synchronous polar winter starphotometry and lidar measurements at a High Arctic station, Atmos. Meas. Tech., 8, 3789–3809, doi:10.5194/amt-8-3789-2015, 2015. 11082, 11083

Barreto, A., Cuevas, E., Damiri, B., Guirado, C., Berkoff, T., Berjón, A. J., Hernández, Y., Almansa, F., and Gil, M.: A new method for nocturnal aerosol measurements with a lunar photometer prototype, Atmos. Meas. Tech., 6, 585–598, doi:10.5194/amt-6-585-2013, 2013. 11082, 11083, 11084, 11090, 11091

Barreto, A., Cuevas, E., Damiri, B., Romero, P. M., and Almansa, F.: Column water vapor determination in night period with a lunar photometer prototype, Atmos. Meas. Tech., 6, 2159–2167, doi:10.5194/amt-6-2159-2013, 2013. 11082, 11083, 11084, 11094, 11107

Barreto, A., Cuevas, E., Mortier, A., Goloub, P., Podvin, T., Blarel, L., Choliy, V., and Hernández, Y.: Nighttime characterization of AOD and water vapor using lunar photometry, Synergies

AMTD
8, 11077–11138, 2015

The new sun-sky-lunar Cimel CE318-T multiband photometer

A. Barreto et al.

with Lidar technique, WMO-TECO/CIMO-16, Commission for Instruments and Methods of Observations (CIMO), St. Petesburg, Russian Federation, 7–9 July, 2014. 11083

Barreto, A., Cuevas, E., Pallé, P., Romero, P. M., Guirado, C., Wehrli, C. J., and Almansa, F.: Recovering long-term aerosol optical depth series (1976–2012) from an astronomical potassium-based resonance scattering spectrometer, Atmos. Meas. Tech., 7, 4103–4116, doi:10.5194/amt-7-4103-2014, 2014. 11087

Berk, A., Anderson, G. P., Bernstein, L. S., Acharya, P. K., Dothe, H., Matthew, M. W., Adler-Golden, S. M., Chetwynd, J. H. J., Richtsmeier, S. C., Pukall, B., Allred, C. L., Jeong, L. S., and Hoke, M. L..: MODTRAN4 Radiative Transfer Modelling for Atmospheric Correction, SPIE Proceeding on Optical Spectroscopic Techniques and Instrumentation for Atmospheric and Space Research, III, 3756, 348–353, 1999. 11094

Bravo-Aranda, J. A., Titos, G., Granados-Muñoz, M. J., Guerrero-Rascado, J. L., Navas-Guzmán, F., Valenzuela, A., Lyamani, H., Olmo, F. J., Andrey, J., and Alados-Arboledas, L.: Synergetic analysis of remote sensing and in-situ data for tracking the interaction mechanisms between Saharan dust and the planetary boundary layer, Tellus B, accepted, 2015. 11087

Bruegge, C. J., Conel, J. E., Green, R. O., Margolis, J. S., Holm, R. G., and Toon, G.: Water vapor column abundances retrievals during FIFE, J. Geophys. Res., 97, 18759–18768, 1992. 11093

Campbell, J. R., Hlavka, D. L., Welton, E. J., Flynn, C. J., Turner, D. D., Spinhirne, J. D., Scott, V. S., and Hwang, I. H.: Full-time, Eye-Safe Cloud and Aerosol Lidar Observation at Atmospheric Radiation Measurement Program Sites: Instrument and Data Processing, J. Atmos. Oceanic Technol., 19, 431–442, 2002. 11089

Chaikovsky, A., Dubovik, O., Goloub, P., Tanré, D., Pappalardo, G.,Wandinger, U., Chaikovskaya, L., Denisov, S., Grudo, Y., Lopatsin, A., Karol, J., Lapyonok, T., Korol, M., Osipenko, F., Savitski, D., Slesar, A., Apituley, A., Alados-Arboledas, L., Binietoglou, I., Kokkalis, P., Granados-Muñoz, M. J., Papayannis, A., Perrone, M. R., Pietruczuk, A., Pisani, G., Rocadenbosch, F., Sicard, M., De Tomasi, F., Wagner, J., and Wang, X.: Algorithm and software for the retrieval of vertical aerosol properties using combined lidar/radiometer data: dissemination in EARLINET, Reviewed Revised Papers of the 26th International Laser Radar Conference, 25–29 June, Porto Heli, Greece, Paper SO3-09, 2012. 11082, 11083

Cuesta, J., Flamant, H. P., and Flamant, C.: Synergetic technique combining elastic backscatter lidar data and sunphotometer AERONET inversion for retrieval by layer of aerosol optical and microphysical properties, Appl. Optics, 47, 4598–4611, 2008. 11082, 11109

Cuevas, E., González, Y., Rodríguez, S., Guerra, J. C., Gómez-Peláez, A. J., Alonso-Pérez, S., Bustos, J., and Milford, C.: Assessment of atmospheric processes driving ozone variations in the subtropical North Atlantic free troposphere, Atmos. Chem. Phys., 13, 1973–1998, doi:10.5194/acp-13-1973-2013, 2013. 11087

Cuevas, E., Camino, C., Benedetti, A., Basart, S., Terradellas, E., Baldasano, J. M., Morcrette, J. J., Marticorena, B., Goloub, P., Mortier, A., Berjón, A., Hernández, Y., Gil-Ojeda, M., and Schulz, M.: The MACC-II 2007–2008 reanalysis: atmospheric dust evaluation and characterization over northern Africa and the Middle East, Atmos. Chem. Phys., 15, 3991–4024, doi:10.5194/acp-15-3991-2015, 2015. 11087

Dach, R., Hugentobler, U., Fridez, P., and Meindl, M.: Bernese GPS Software Version 5.0, Astronomical Institute, University of Bern, Switzerland, available at: http://www.bernese.unibe.ch/docs50/DOCU50.pdf, 2007. 11089

Eck, T., Holben, B., Reid, J. S., Dubovik, O., Smirnov, A., O'Neill, N. T., Slutsker, I., and Kinne, S.: Wavelength dependence of the optical depth of biomass burning urban and desert dust aerosols, J. Geophys. Res., 104, 31333–31349, doi:10.1029/1999JD900923, 1999. 11095, 11103, 11105

Fernald, F. G.: Analysis of atmospheric lidar observations – Some comments, Appl. Optics, 23, 652–653, 1984. 11082, 11083

Forster, P., Ramaswamy, V., Artaxo, P., Berntsen, T., Betts, R., Fahey, D. W., Haywood, J., Lean, J., Lowe, D. C., Myhre, G., Nganga, J., Prinn, R., Raga, G., Schulz, M., and Van Dorland, R.: Changes in Atmospheric Constituents and in Radiative Forcing, in: Climate Change 2007: The Physical Science Basis. Contribution of Working Group I to the Fourth Assessment Report of the Intergovernmental Panel on Climate Change, edited by: Solomon S., Qin, D., Manning, M., Chen, Z., Marquis, M., Averyt, K. B., Tignor, M., and Miller, H. L., Cambridge University Press, Cambridge, UK and New York, NY, USA, 129–234, 2007. 11080

Granados-Muñoz, M. J., Guerrero-Rascado, J. L., Bravo-Aranda, J. A., Navas-Guzmán, F., Valenzuela, A., Lyamani, H., Chaikovsky, A., Wandinger, U., Ansmann, A., Dubovik, O., Grudo, J. O., and Alados-Arboledas, L.: Retrieving aerosol microphysical properties by Lidar Radiometer Inversion Code (LIRIC) for different aerosol types, J. Geophys. Res.-Atmos., 119, 4836–4858, 2014. 11083

Gröbner, J., Kouremeti, N., de Coulon, E., Dürig, F., Gyo, M., Soder, R., and Waser, D.: Spectroradiometer for Spectral Aerosol Optical Depth and Solar Irradiance Measurements, Annual Report PMOD, p. 13, 2012, http://www.pmodwrc.ch/annual_report/annualreport2012.pdf, 2012. 11088

Guerrero-Rascado, J. L., Olmo, F. J., Avilés-Rodríguez, I., Navas-Guzmán, F., Pérez-Ramírez, D., Lyamani, H., and Alados Arboledas, L.: Extreme Saharan dust event over the southern Iberian Peninsula in september 2007: active and passive remote sensing from surface and satellite, Atmos. Chem. Phys., 9, 8453–8469, doi:10.5194/acp-9-8453-2009, 2009. 11087

Guirado, C., Cuevas, E., Cachorro, V. E., Toledano, C., Alonso-Pérez, S., Bustos, J. J., Basart, S., Romero, P. M., Camino, C., Mimouni, M., Zeudmi, L., Goloub, P., Baldasano, J. M., and de Frutos, A. M.: Aerosol characterization at the Saharan AERONET site Tamanrasset, Atmos. Chem. Phys., 14, 11753–11773, doi:10.5194/acp-14-11753-2014, 2014. 11109

JCGM: JCGM 100:2008, GUM 1995 with Minor Corrections, Evaluation of Measurement Data – guide to the Expression of Uncertainty in Measurement, Joint Committee for Guides in Metrology, Member organizations: BIPM, IEC, IFCC, ILAC, ISO, IUPAC, IUPAP, and OIML, 2008. 11094

Halthore, R. N., Eck, T. F., Holben, B. N., and Markham, B. L.:Sun photometric measurements of atmospheric water vapor column abundance in the 940-nm band, J. Geophys. Res., 102, 4343–4352, 1997. 11093

Herber, A., Thomason, L. W., Gernandt, H., Leiterer, U., Nagel, D., Schulz, K.-H., Kaptur, J., Albrecht, T., and Notholt, J.: Continuous day and night aerosol optical depth observations in the Arctic between 1991 and 1999, J. Geophys. Res.-Atmos., 107, AAC6.1–AAC6.13, doi:10.1029/2001JD000536, 2002. 11082

Hoffmann, A., Ritter, C., Stock, M., Shiobara, M., Lampert, A., Maturilli, M., Orgis, T., Neuber, R., and Herber, A.: Ground-based lidar measurements from Ny-Ålesund during ASTAR 2007, Atmos. Chem. Phys., 9, 9059–9081, doi:10.5194/acp-9-9059-2009, 2009. 11082

Holben, B. N., Eck, T. F., Slutsker, I., Tanré, D., Buis, J. P., Setzer, A., Vermote, E., Reagan, J. A., Kaufman, Y. J., Nakajima, T., Lavenu, F., Jankowiak, I., and Smirnov A.: AERONET – A federated instrument network and data archive for aerosol characterization, Remote Sens. Environ., 66, 1–16, 1998. 11081, 11083, 11084, 11087, 11088, 11091, 11094, 11095, 11097

Holben, B. N., Tanré, D., Smirnov, A., Eck, T. F., Slutsker, I., Abuhassan, N., Newcomb, W. W., Schafer, J. S., Chatenet, B., Lavenu, F., Kaufman, Y. J., Vande Castle, J., Setzer, A., Markham, B., Clark, D., Frouin, R., Halthore, R., Karneli, A., O'Neill, N. T., Pietras,

AMTD
8, 11077–11138, 2015

The new sun-sky-lunar Cimel CE318-T multiband photometer

A. Barreto et al.

C., Pinker, R. T., Voss, K., and Zibordi, G.: An emerging ground-based aerosol climatology: Aerosol Optical Depth from AERONET, J. Geophys. Res.-Atmos., 106, 12067–12097, doi:10.1029/2001JD900014, 2001. 11081

Kaufman Y. J., Gitelson, A., Karnieli, A., Ganor, E., and Fraser, R. S.: Size distribution and phase function of aerosol particles retrieved from sky brightness measurements, J. Geophy. Res.-Atmos., 99, 10331–10356, 1994. 11093

Kaufman, Y., Tanré, D., and Boucher, O.: A satellite view of aerosols in the climate system, Nature, 419, 215–223, 2002. 11080

Kazadzis, S., Veselovskii, I., Amiridis, V., Gröbner, J., Suvorina, A., Nyeki, S., Gerasopoulos, E., Kouremeti, N., Taylor, M., Tsekeri, A., and Wehrli, C.: Aerosol microphysical retrievals from precision filter radiometer direct solar radiation measurements and comparison with AERONET, Atmos. Meas. Tech., 7, 2013–2025, doi:10.5194/amt-7-2013-2014, 2014. 11103, 11104

Kieffer, H. H. and Stone, T. C.: The spectral irradiance of the moon, The Astronomical Journal, 129, 2887–2901, 2005. 11090, 11091, 11096

Klett, J. D.: Inversion with variable backscatter/extinction ratios, Appl. Optics, 11, 1638–1643, 1985. 11082, 11083

Lyamani, H., Olmo, F. J., and Alados-Arboledas, L.: Physical and optical properties of aerosols over an urban location in Spain: seasonal and diurnal variability, Atmos. Chem. Phys., 10, 239–254, doi:10.5194/acp-10-239-2010, 2010. 11087

Lyamani, H., Fernández-Gálvez, J., Pérez-Ramírez, D., Valenzuela, A., Antón, M., Alados, I., Titos, G., Olmo, F. J., and Alados-Arboledas, L.: Aerosol properties over two urban sites in South Spain during an extended stagnation episode in winter season, Atmos. Environ., 62, 424–432, 2012. 11087

Lopatin, A., Dubovik, O., Chaikovsky, A., Goloub, P., Lapyonok, T., Tanré, D., and Litvinov, P.: Enhancement of aerosol characterization using synergy of lidar and sun-photometer coincident observations: the GARRLiC algorithm, Atmos. Meas. Tech., 6, 2065–2088, doi:10.5194/amt-6-2065-2013, 2013. 11082, 11083

Myhre, G.: Consistency Between Satellite-Derived and Modeled Estimates of the Direct Aerosol Effect, Science 325, 187, doi:10.1126/science.1174461, 2009. 11080, 11081

Navas-Guzmán, F., Bravo-Aranda, J. A., Guerrero-Rascado, J. L., Granados-Muñoz, M. J., and Alados-Arboledas, L.: Statistical analysis of aerosol optical properties retrieved by Raman lidar over Southeastern Spain, Tellus B, 65, 21234, 2013. 11087

Nyeki, S., Gröbner, J., and Wehrli, C.: Ground-based aerosol optical depth intercomparison campaigns at European EUSAAR super-sites, AIP Conf. Proc., 1531, 584, doi:10.1063/1.4804837, 2013. 11103

Ortiz de Galisteo, J. P., Toledano, C., Cachorro, V. E., and Torres, B.: Improvement in PWV estimation from GPS due to the absolute calibration of antenna phase center variation, GPS Solut., 14, 389–395, doi:10.1007/s10291-010-0163-y, 2010. 11109

Pahlow, M., Müller, D., Tesche, M., Eichler, H., Feingold, G., Eberhard, W. L., and Cheng, Y.: Retrieval of aerosol properties from combined multiwavelength lidar and Sun photometer measurements, Appl. Opt., 45, 7429–7442, doi:10.1364/AO.45.007429, 2006. 11083

Pappalardo, G., Amodeo, A., Apituley, A., Comeron, A., Freudenthaler, V., Linné, H., Ansmann, A., Bösenberg, J., D'Amico, G., Mattis, I., Mona, L., Wandinger, U., Amiridis, V., Alados-Arboledas, L., Nicolae, D., and Wiegner, M.: EARLINET: towards an advanced sustainable European aerosol lidar network, Atmos. Meas. Tech., 7, 2389–2409, doi:10.5194/amt-7-2389-2014, 2014.

Pérez-Ramírez, D., Ruiz, B., Aceituno, J., Olmo, F. J., and Alados-Arboledas, L.: Application of Sun/star photometry to derive the aerosol optical depth, Int. J. Remote Sens., 29, 5113–5132, doi:10.1080/01431160802036425, 2008. 11082

Pérez-Ramírez, D., Aceituno, J., Ruiz, B., Olmo, F. J., and Alados-Arboledas, L.: Development and calibration of a star-photometer to measure the aerosol optical depth: Smoke observations at a high mountain site, Atmos. Environ., 42, 2733–2738, 2008. 11088

Pérez-Ramírez, D., Lyamani, H., Olmo, F. J., and Alados-Arboledas, L.: Improvements in star photometry for aerosol characterizations, J. Aerosol Sci., 42, 737–745, doi:10.1016/j.jaerosci.2011.06.010, 2011. 11082, 11088, 11104

Pérez-Ramírez, D., Lyamani, H., Olmo, F. J., Whiteman, D. N., Navas-Guzmán, F., and Alados-Arboledas, L.: Cloud screening and quality control algorithm for star photometer data: assessment with lidar measurements and with all-sky images, Atmos. Meas. Tech., 5, 1585–1599, doi:10.5194/amt-5-1585-2012, 2012a. 11088

Pérez-Ramírez, D., Lyamani, H., Olmo, F. J., Whiteman, D. N., and Alados-Arboledas, L.: Columnar aerosol properties from sun-and-star photometry: statistical comparisons and day-to-night dynamic, Atmos. Chem. Phys., 12, 9719–9738, doi:10.5194/acp-12-9719-2012, 2012b. 11088

Pérez-Ramírez, D., Veselovskii, I., Whiteman, D. N., Suvorina, A., Korenskiy, M., Kolgotin, A., Holben, B., Dubovik, O., Siniuk, A., and Alados-Arboledas, L.: High temporal resolution estimates of columnar aerosol microphysical parameters from spectrum of aerosol optical depth by linear estimation: application to long-term AERONET and star-photometry measurements, Atmos. Meas. Tech., 8, 3117–3133, doi:10.5194/amt-8-3117-2015, 2015. 11088

Rodríguez, S., Alastuey, A., Alonso-Pérez, S., Querol, X., Cuevas, E., Abreu-Afonso, J., Viana, M., Pérez, N., Pandolfi, M., and de la Rosa, J.: Transport of desert dust mixed with North African industrial pollutants in the subtropical Saharan Air Layer, Atmos. Chem. Phys., 11, 6663–6685, doi:10.5194/acp-11-6663-2011, 2011. 11087

Rodríguez, S., Cuevas, E., Prospero, J. M., Alastuey, A., Querol, X., López-Solano, J., García, M. I., and Alonso-Pérez, S.: Modulation of Saharan dust export by the North African dipole, Atmos. Chem. Phys., 15, 7471–7486, doi:10.5194/acp-15-7471-2015, 2015. 11087

Romero, P. M., Cuevas, E., Ramos, R., Valdés, M., and Schneider, M.: Programa de vapor de agua en columna del Centro de Investigación Atmosférica de Izaña: análisis e intercomparación de diferentes técnicas de medida, NIPO: 784-09-009-9, Agencia Estatal de Meteorología, Ministerio de Medio Ambiente, y Medio Rural y Marino, Madrid, Spain, 2009. 11089

Sasano, Y., Browell, E. V., and Ismail, S.: Error caused by using a constant extinction backscattering ratio in the lidar solution, Appl. Optics, 24, 3929–3932, 1985. 11083

Schmid, B., Thome, K. J., Demoulin, P., Peter, R., Mätzler, C., and Sekler, J.: Comparison of modeled and empirical approaches for retrieving columnar water vapor from solar transmittance measurements in the 0.94-µm region, J. Geophys. Res., 101, 9345–9358, 1996. 11093

Schmid, B., Michalsky, J., Halthore, R., Beauharnois, M., Harisson, L., Livingston, J., Russell, P., Holben, B., Eck, T., and Smirnov, A.: Comparison of aerosol optical depth from four solar radiometers during the fall 1997 ARM intensive observation period, J. Geophys. Res., 26, 2725–2728, 1999. 11095, 11105

Schneider, M., Romero, P. M., Hase, F., Blumenstock, T., Cuevas, E., and Ramos, R.: Continuous quality assessment of atmospheric water vapour measurement techniques: FTIR, Cimel, MFRSR, GPS, and Vaisala RS92, Atmos. Meas. Tech., 3, 323–338, doi:10.5194/amt-3-323-2010, 2010. 11107

Smirnov, A., Holben, B. N., Slutsker, I., Welton, E, J., and Formenti, P.: Optical properties of Saharan dust during ACE 2, J. Geophys. Res., 103, 28079–28092, doi:10.1029/98JD01930, 1998. 11108

Spinhirne, J. D., Rall, J. A. R., and Scott, V. S.: Compact Eye Safe Lidar Systems, Rev. Laser Eng., 23, 112–118, 1995. 11089

Stocker, T. F., Qin, D., Plattner, G.-K., Tignor, M., Allen, S. K., Boschung, J., Nauels, A., Xia, Y., Bex, V., and Midgley, P. M.: Climate Change 2013: The Physical Science Basis. Contribution of Working Group I to the Fifth Assessment Report of the Intergovernmental Panel on Climate Change, Cambridge University Press, Cambridge, United Kingdom and New York, NY, USA, 1535 pp., doi:10.1017/CBO9781107415324, 2013. 11080

Suparta, W., Mohd. Ali, M. A., Yatim, B., and Fraser, G. J.: Analysis of GPS-sensed atmospheric water vapour variability and its response to the terrestrial winds over Antarctica, Phys. Chem. Earth, 34, 72–87, 2009. 11109

Tesche, M., Müller, D., Ansmann, A., Hu, M., and Zhang, Y.: Retrieval of microphysical properties of aerosol particles from one-wavelength Raman lidar and multiwavelength sun photometer observations, Atmos. Environ., 42, 6398–6404, doi:10.1016/j.atmosenv.2008.02.014, 2008. 11083

Titos, G., Lyamani, H., Pandolfi, M., Alastuey, A., and Alados-Arboledas, L.: Identification of fine (PM1) and coarse (PM10-1) sources of particulate matter in an urban environment, Atmos. Environ., 89, 593–602, 2014. 11087

Tomasi, C., Kokhanovsky, A. A., Lupi, A., Ritter, C., Smirnov, A., O'Neill, N. T., Stone, R. S., Holben, B. N., and Nyeki, S.: Aerosol remote sensing in polar regions, Earth-Sci. Rev., 140, 108–157, doi:10.1016/j.earscirev.2014.11.001, 2015. 11082

Toledano, C., Cachorro, V. E., Berjón, de Frutos, A. M., Sorribas, M., de la Morena, B. A., and Goloub, P.: Aerosol optical depth and Angström exponent climatology at El Arenosillo AERONET site (Huelva, Spain), Q. J. Roy. Meteorol. Soc., 133, 795–807, doi:10.1002/qj.54, 2007. 11095

Valenzuela, A., Olmo, F. J., Lyamani, H., Antón, M., Quirantes, A., and Alados-Arboledas, L.: Classification of aerosol radiative properties during African desert dust intrusions over southeastern Spain by sector origins and cluster analysis, J. Geophys. Res.-Atmos., 117, D06214, doi:10.1029/2011JD016885, 2012. 11087

Wagner, J., Ansmann, A., Wandinger, U., Seifert, P., Schwarz, A., Tesche, M., Chaikovsky, A., and Dubovik, O.: Evaluation of the Lidar/Radiometer Inversion Code (LIRIC) to determine microphysical properties of volcanic and desert dust, Atmos. Meas. Tech., 6, 1707–1724, doi:10.5194/amt-6-1707-2013, 2013. 11083

Welton E. J. and Campbell J. R.: Micropulse Lidar Signals: Uncertainty Analysis, J. Atmos. Oceanic Technol., 19, 2089–2094, 2002. 11089

Wehrli, C.: Calibrations of filter radiometers for determination of atmospheric optical depth, Metrología, 37, 419–422, 2000. 11081

Wehrli, C.: GAW-PFR: A network of Aerosol Optical Depth observations with Precision Filter Radiometers, in: WMO/GAW Experts workshop on a global surface based network for long term observations of column aerosol optical properties, GAW Report No. 162, WMO TD No. 1287, 2005. 11081

WMO/GAW aerosol measurements procedures guidelines and recommendations, WMO report no. 153, TD No. 1178, September 2003. 11081

WMO/GAW Experts workshop on a global surface-based network for long term observations of column aerosol optical properties, edited by: Baltensperger, U., Barrie, L., and Wehrli, C., GAW No. 162, WMO/TD-No. 1287, 2005. 11102, 11103

Wu, P., Hamada, J.-I., Mori, S., Tauhid, Y. I., Yamanaka, M. D., and Kimura, F.: Diurnal Variation of Precipitable Water over a Mountainous Area of Sumatra Island, J. Appl. Meteor., 42, 1107–1115, 2003. 11109

AMTD

8, 11077–11138, 2015

The new sun-sky-lunar Cimel CE318-T multiband photometer

A. Barreto et al.

Table 1. Statistics of the master vs. secondary AOD comparison: mean bias (MB), root mean square error (RMSE) and Pearson correlation coefficient (r).

DAYLIGHT ($N = 5566$)						
Channel (nm)	1020	1640	870	675	440	500
MB	0.001	0.002	0.001	0.001	0.001	0.002
RMSE	0.002	0.002	0.002	0.002	0.000	0.002
r	0.999	0.999	0.999	0.999	0.999	0.999
NIGHTTIME -Sun Ratio- ($N = 2319$)						
MB	−0.004	0.001	−0.001	−0.002	−0.002	−0.001
RMSE	0.006	0.003	0.003	0.004	0.008	0.005
r	0.996	0.999	0.998	0.998	0.992	0.996
NIGHTTIME -Moon Ratio- ($N = 2319$)						
MB	−40.001	0.000	−0.001	−0.000	−0.001	−0.000
RMSE	0.005	0.002	0.003	0.003	0.007	0.005
r	0.996	0.999	0.998	0.998	0.992	0.996

AMTD
8, 11077–11138, 2015

Table 2. Statistics of the CE318-T and star photometer AOD comparison during August 2014: mean bias (MB), root mean square error (RMSE), Pearson correlation coefficient (r) and number of coincidences (N).

Channel (nm)	870	500	440
MB	−0.001	0.013	−0.033
RMSE	0.003	0.009	0.018
r	0.946	0.937	0.911
N	15	15	14

AMTD
8, 11077–11138, 2015

Table 3. MB and RMSE values for AOD differences between CE318-AERONET daytime and CE318-T nighttime data during sunset-moonrise (SS-MR, defined as the last 1 h of daytime data versus the first 1 h of nocturnal data) as a function of the average moon's fraction of illumination (FI).

			SS-MR					
	# cases		1020	1640	870	675	500	440
60 % ≥ FI > 50 %	2	MB	0.035	0.061	0.012	−0.015	−0.008	−0.019
		RMSE	0.037	0.062	0.017	0.018	0.014	0.022
70 % ≥ FI > 60 %	2	MB	0.029	0.051	0.008	−0.014	−0.007	−0.015
		RMSE	0.029	0.051	0.009	0.014	0.008	0.016
80 % ≥ FI > 70 %	1	MB	0.048	0.056	0.024	0.008	0.016	0.006
		RMSE	–	–	–	–	–	–
90 % ≥ FI > 80 %	4	MB	0.016	0.027	0.001	−0.010	−0.012	−0.016
		RMSE	0.018	0.027	0.003	0.011	0.013	0.016
95 % ≥ FI > 90 %	3	MB	0.001	0.010	−0.004	−0.010	−0.016	−0.016
		RMSE	0.003	0.010	0.006	0.012	0.017	0.017
FI ≥ 95 %	8	MB	0.015	0.009	0.014	0.013	0.010	0.012
		RMSE	0.008	0.006	0.008	0.008	0.008	0.008

AMTD
8, 11077–11138, 2015

The new sun-sky-lunar Cimel CE318-T multiband photometer

A. Barreto et al.

Table 4. MB and RMSE values for AOD differences between CE318-AERONET daytime and CE318-T nighttime data during moonset-sunrise (MS-SR, as the first 1 h of daytime data versus the last 1 h of nocturnal data) as a function of the average moon's fraction of illumination (FI).

			MS-SR					
	# cases		1020	1640	870	675	500	440
50 % ≥ FI > 60 %	1	MB	0.012	0.046	0.003	−0.009	−0.008	−0.006
		RMSE	–	–	–	–	–	–
60 % ≥ FI > 70 %	1	MB	0.007	0.039	−0.002	−0.014	−0.005	−0.015
		RMSE	–	–	–	–	–	–
80 % ≥ FI > 70 %	2	MB	0.007	0.034	−0.001	−0.012	−0.012	−0.017
		RMSE	0.010	0.034	0.003	0.012	0.013	0.017
90 % ≥ FI > 80 %	4	MB	0.012	0.023	0.009	0.002	−0.001	−0.001
		RMSE	0.002	0.012	0.001	0.006	0.009	0.009
95 % ≥ FI > 90 %	4	MB	0.011	0.016	0.007	−0.002	−0.002	−0.001
		RMSE	0.015	0.018	0.011	0.009	0.011	0.010
FI ≥ 95 %	11	MB	−0.001	−0.003	−0.002	−0.004	−0.009	−0.006
		RMSE	0.002	0.004	0.002	0.004	0.008	0.006

AMTD
8, 11077–11138, 2015

AMTD
8, 11077–11138, 2015

Table 5. Main statistics of the PWV comparison (in cm) extracted from CE318-T, CE318-AERONET and GNSS for daytime data, and from CE318-T and GNSS for nocturnal data. In case of nighttime information a comparison in function of the moon's fraction of illumination (FI, in %) is also included.

	DAY			
Instruments	MB	RMSE	r	N
CE318-T/CE318-AERONET	−0.02	0.02	0.99	1935
CE318-T/GNSS	−0.09	0.05	0.97	461
	NIGHT			
CE318-T/GNSS	MB	RMSE	r	N
60% ≥ FI > 50 %	−0.08	0.09	0.99	10
70% ≥ FI > 60 %	−0.07	0.08	0.99	10
80% ≥ FI > 70 %	−0.01	0.02	0.98	10
90% ≥ FI > 80 %	−0.03	0.07	0.99	43
95% ≥ FI > 90 %	−0.03	0.06	0.98	41
100% ≥ FI > 95 %	−0.02	0.05	0.99	93
TOTAL				207

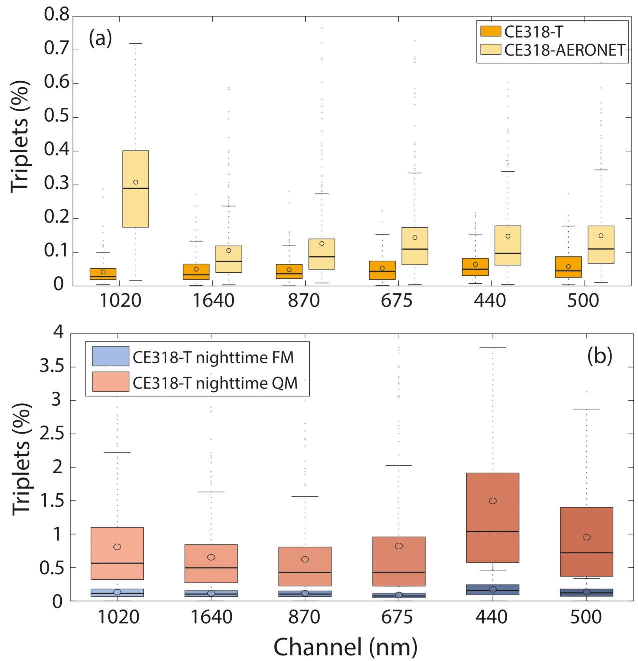

Figure 1. Boxplot of triplets (in %) measured at IZO for **(a)** CE318-T and CE318-AERONET in a daytime period of 23 days from February and March 2015, with pristine conditions (AOD at 500 nm $\leq$ 0.02), and **(b)** for CE318-T in a nighttime period of seven nights near full moon (FM, in blue) and five nights near quarter moon (QM, in red) between January and April 2015. In this figure circles represent the mean value while the horizontal line inside each box is the median value.

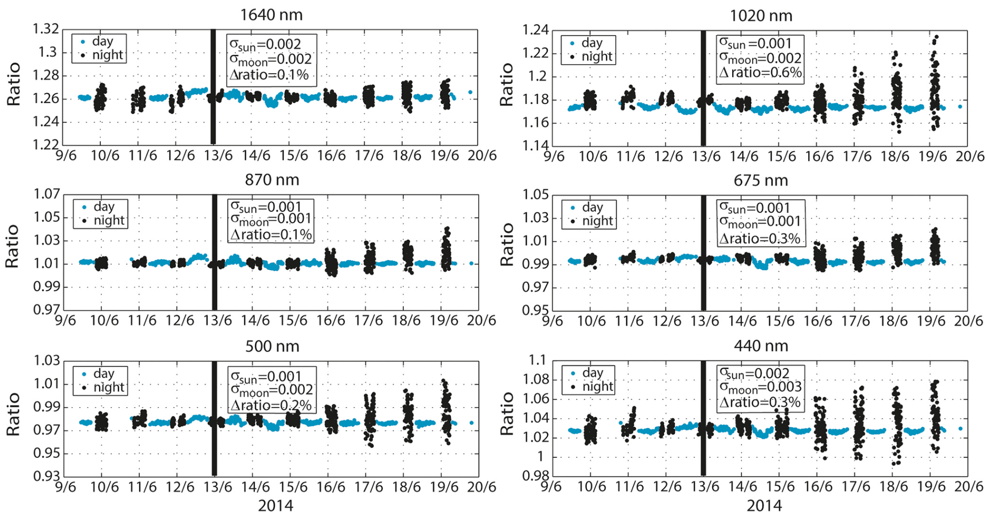

Figure 2. Ratio of simultaneous master/secondary signals at IZO performed in 11 consecutive days and 10 consecutive nights in June 2014. Vertical black line corresponds to the coincidence of full moon conditions. Standard deviations (σs) and ratio differences (Δ ratio) are depicted in each figure for sun midday and ±1 night near full moon events ratios.

AMTD
8, 11077–11138, 2015

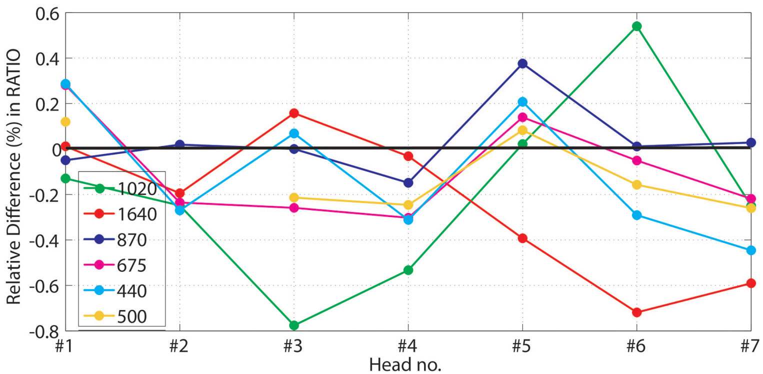

Figure 3. Relative differences between $Ratio_{sun}$ and $Ratio_{moon}$ for seven different heads at IZO.

AMTD
8, 11077–11138, 2015

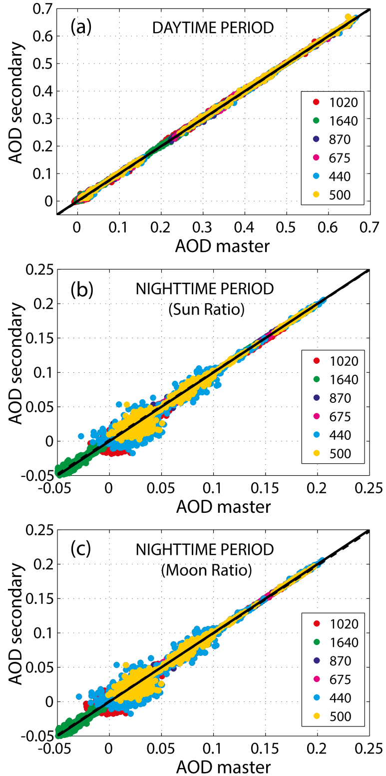

Figure 4. Scatterplot with CE318-T master versus secondary derived AODs for **(a)** a period of 22 consecutive days and **(b)** and **(c)** for a period of 10 consecutive nights in June 2014, with the secondary calibrated using the Sun Ratio and the Moon Ratio techniques, respectively.

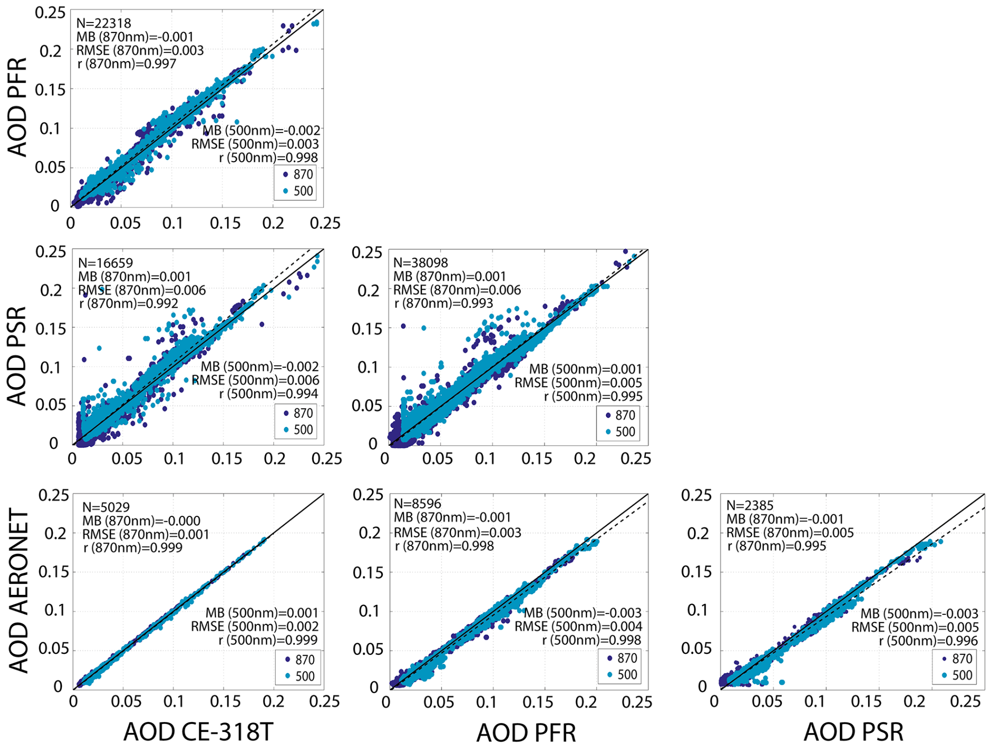

Figure 5. Scatterplots of AOD at 870 nm (blue) and 500 nm (cyan) using four different and independent measurements (CE318-T, CE318-AERONET, PFR and PSR) during March, April, May and June 2014 at IZO. In each figure, the dotted line represents the linear regression line, and the solid line is the diagonal.

AMTD
8, 11077–11138, 2015

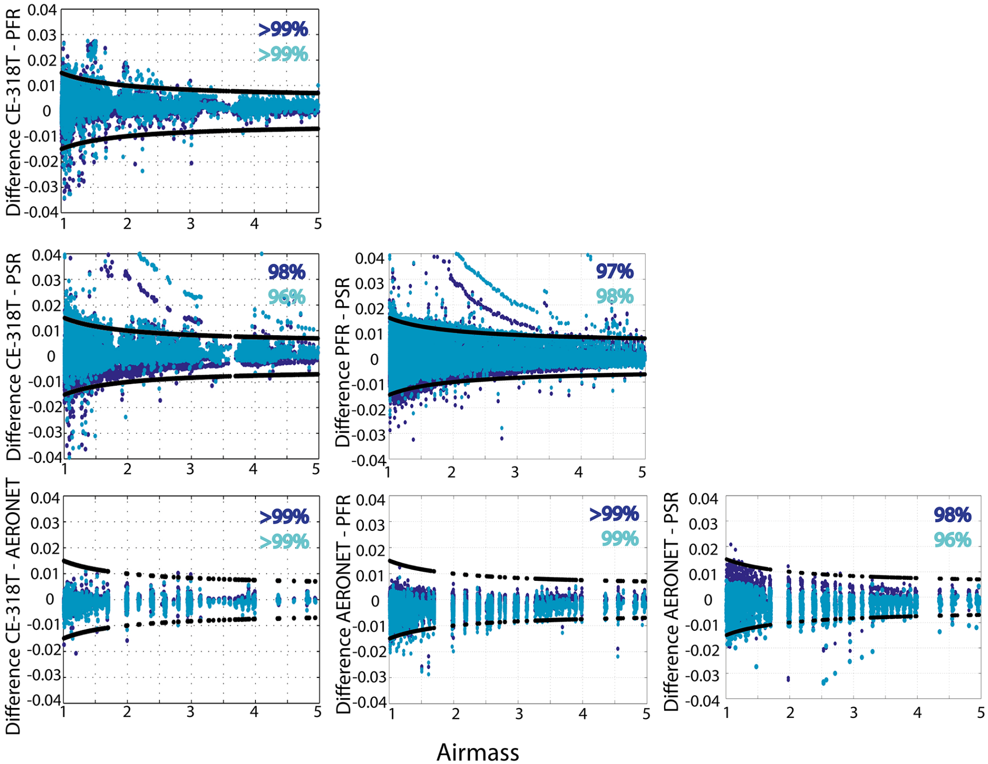

Figure 6. AOD differences versus airmass for channel centered at 870 nm (blue) and 500 nm (cyan). Solid line represents the $U95$ uncertainty limit. In each figure the percentage of points within the $U95$ limits is included.

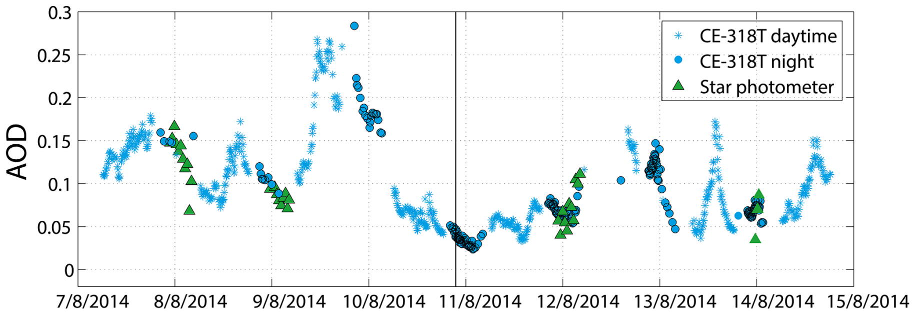

Figure 7. AOD at 500 nm channel from CE318-T at daytime and nighttime (in blue), and from the star photometer (in green) at Granada in eight consecutive days in August 2014. Vertical line represents the full moon phase.

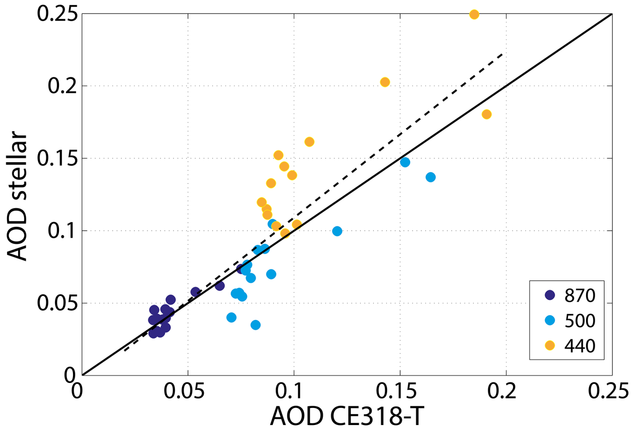

Figure 8. Scatterplot CE318-T AOD versus stellar AOD at Granada for four nights in August 2014. The dotted line represents the linear regression line, and the solid line is the 1 : 1 line.

AMTD
8, 11077–11138, 2015

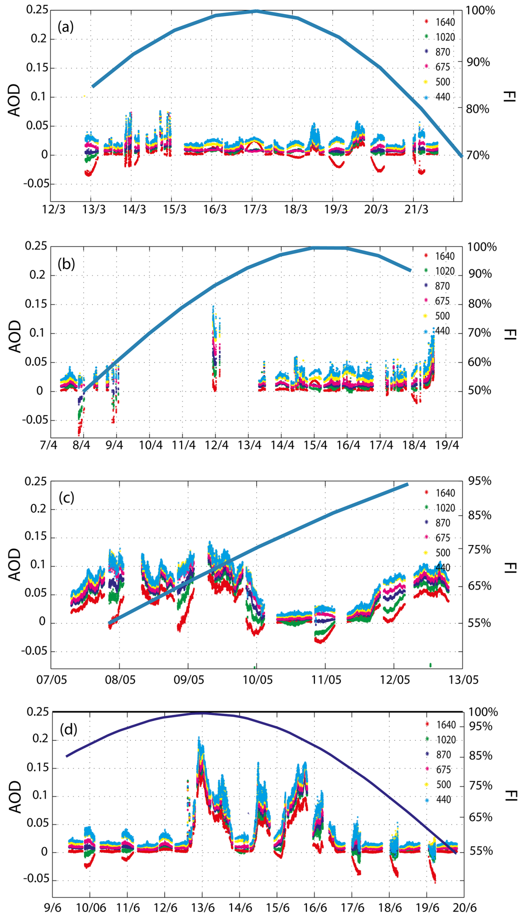

Figure 9. Diurnal CE318-AERONET/CE318-T AOD evolution during **(a)** March, **(b)** April, **(c)** May and **(d)** June 2014 at IZO. The blue line and right y-axis correspond to the evolution in this period of the moon's factor of illumination (FI).

AMTD
8, 11077–11138, 2015

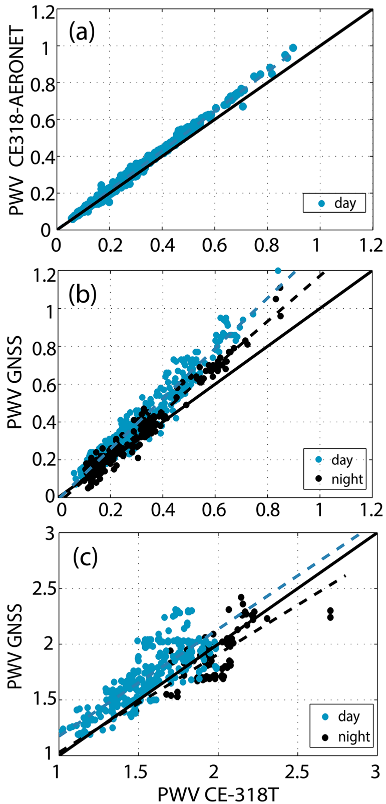

Figure 10. Scatterplot with daytime (in blue) master CE318-T PWV (in cm) vs. **(a)** CE318-AERONET, **(b)** daytime and nighttime master (black) CE318-T PWV's (in cm) vs. GNSS, and **(c)** daytime and nighttime PWV comparison performed at Granada station using the secondary CE318-T and GNSS ultra-rapid orbits. The dotted line represents in all figures the linear regression line and the solid line the 1 : 1 line.

AMTD
8, 11077–11138, 2015

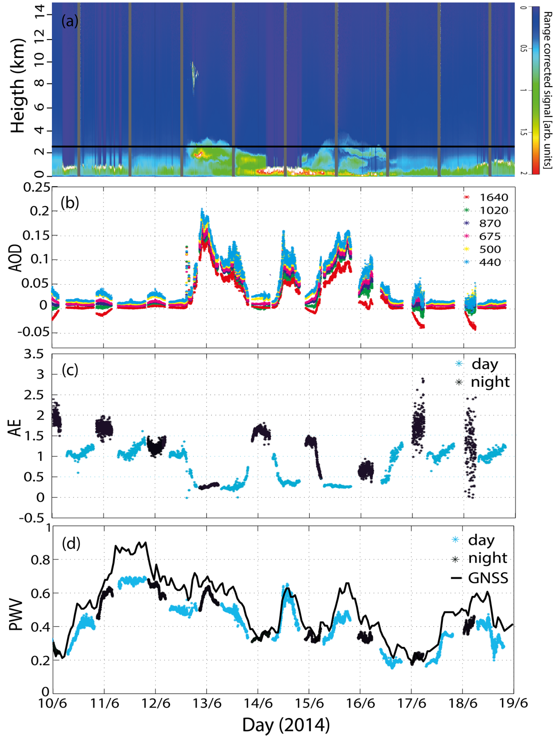

Figure 11. Case study at IZO in June, 2014, including information for **(a)** MPL corrected backscatter cross-section obtained from Santa Cruz de Tenerife station (60 m a.s.l.). Black horizontal line represents the altitude of IZO station. Grey vertical lines represent the absence of measurements. The CE318-T AOD, AE and PWV evolution from 10 to 19 June, 2014 are shown in **(b)**, **(c)** and **(d)**. PWV values from GNSS precise orbits are plotted with a black solid line.

AMTD
8, 11077–11138, 2015

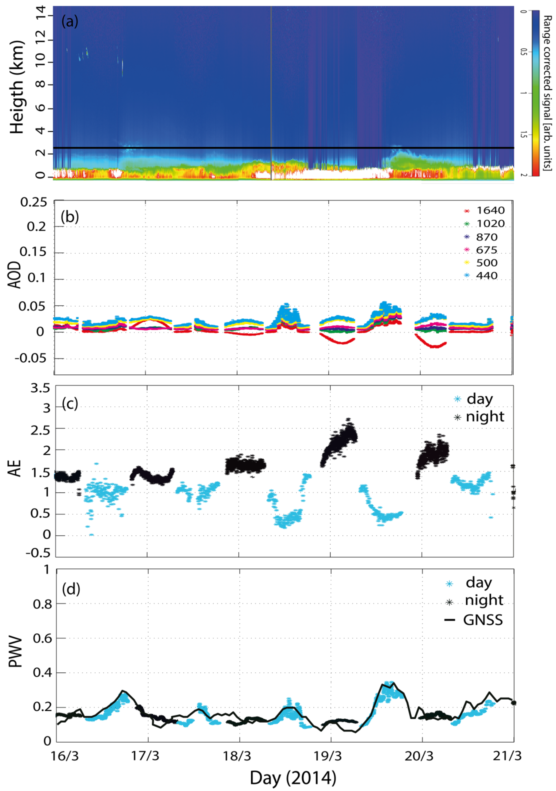

Figure 12. Case study at IZO in March 2014, including information for **(a)** MPL corrected backscatter cross-section obtained from Santa Cruz de Tenerife station (60 m a.s.l.). Black horizontal line represents the altitude of IZO station. Grey vertical lines represent the absence of measurements. The CE318-T AOD, AE and PWV evolution from 16 to 21 March, 2014 are shown in **(b)**, **(c)** and **(d)**. PWV values from GNSS precise orbits are plotted with a black solid line.

AMTD
8, 11077–11138, 2015

Title Page
Abstract | Introduction
Conclusions | References
Tables | Figures
◀I | ▶I
◀ | ▶
Back | Close
Full Screen / Esc
Printer-friendly Version
Interactive Discussion